



8-2009

# Airplane Piston Engine Dynamics as an Aeronca E-113 Case Study

Michael Charles Leigh  
*University of Tennessee - Knoxville*

---

## Recommended Citation

Leigh, Michael Charles, "Airplane Piston Engine Dynamics as an Aeronca E-113 Case Study." Master's Thesis, University of Tennessee, 2009.  
[https://trace.tennessee.edu/utk\\_gradthes/44](https://trace.tennessee.edu/utk_gradthes/44)

This Thesis is brought to you for free and open access by the Graduate School at Trace: Tennessee Research and Creative Exchange. It has been accepted for inclusion in Masters Theses by an authorized administrator of Trace: Tennessee Research and Creative Exchange. For more information, please contact [trace@utk.edu](mailto:trace@utk.edu).

To the Graduate Council:

I am submitting herewith a thesis written by Michael Charles Leigh entitled "Airplane Piston Engine Dynamics as an Aeronca E-113 Case Study." I have examined the final electronic copy of this thesis for form and content and recommend that it be accepted in partial fulfillment of the requirements for the degree of Master of Science, with a major in Aviation Systems.

U. Peter Solies, Major Professor

We have read this thesis and recommend its acceptance:

Basil N. Antar, Gary A. Flandro

Accepted for the Council:

Dixie L. Thompson

Vice Provost and Dean of the Graduate School

(Original signatures are on file with official student records.)

---

To the Graduate Council:

I am submitting herewith a thesis written by Michael Charles Leigh entitled “Airplane Piston Engine Dynamics as an Aeronca E-113 Case Study.” I have examined the final electronic copy of this thesis for form and content and recommend that it be accepted in partial fulfillment of the requirements for the degree of Master of Science, with a major in Aviation Systems.

---

U. Peter Solies, Major Professor

We have read this thesis and  
recommend its acceptance:

Basil N. Antar

Gary A. Flandro

Accepted for the Council:

Carolyn R. Hodges  
Vice Provost and Dean of the  
Graduate School

(Original signatures are on file with official student records)

Airplane Piston Engine Dynamics  
as an  
Aeronca E-113 Case Study

A Thesis Presented for  
The Master of Science Degree in Aviation Systems  
The University of Tennessee, Knoxville

Michael Charles Leigh  
August 2009

## Dedication

To my daughters Hannah and Piper who give purpose to everything I do.

## Abstract

Kinematic equations were developed to describe the dynamic motions of the aircraft piston engine components in terms of time dependent position, velocity, and acceleration relationships. Using the Aeronca E-113 engine as a case study, the brake mean effective pressure (BMEP) rating was used to model the cylinder gas pressure profile. The moments of inertia of the dynamic components including connecting rod, crankshaft, and propeller were measured using a pendulum swing method. Representative values were obtained for inertial and gas pressure forces acting on crankshaft journals, connecting rods, and cylinder walls. The resulting model can help in the design of crankshafts and other dynamically loaded parts to resist failure due to fatigue.

# Table of Contents

List of Tables . . . . .	v
List of Figures . . . . .	vi
Nomenclature . . . . .	viii
Acronyms . . . . .	x
1.0 Introduction . . . . .	1
1.1 The Aeronca E-113 Airplane Engine . . . . .	5
1.2 Software Tools . . . . .	6
2.0 Component Weights and Inertias . . . . .	7
2.1 Moment of Inertia Calculations . . . . .	7
2.2 Connecting Rod Center of Gravity . . . . .	10
2.3 Counterweight Mass and Inertia . . . . .	11
3.0 Piston Pressures . . . . .	15
4.0 Crank Geometry and Kinematics . . . . .	24
4.1 Piston Kinematics . . . . .	24
4.2 Connecting Rod Kinematics . . . . .	29
4.3 Piston Forces . . . . .	32
4.4 Connecting Rod Forces . . . . .	34
4.5 Crankshaft Forces . . . . .	37
4.6 Shaft Torque . . . . .	41
4.7 Two Cylinder Engine . . . . .	42
4.8 Main Bearing Loads . . . . .	44
5.0 Conclusions . . . . .	46
References . . . . .	48
Appendices. . . . .	53
Appendix A: Dynamometer Data . . . . .	54
Appendix B: Engine Drawings . . . . .	56
Appendix C: Flight Dynamics. . . . .	61
Appendix D: Piston Forces in Dynamic Flight. . . . .	65
Appendix E: MATLAB scripts. . . . .	70
Appendix F: Pictures. . . . .	81
Vita . . . . .	86

## List of Tables

1-1	Aeronca E-113 Engine Specifications . . . . .	5
2-1	Summary of Mass Characteristics of E-113 Engine Components . . . . .	8
2-2	Counterweight Mass Characteristics . . . . .	14
2-3	Counterweight Moment Translation . . . . .	14
2-4	Counterweight Mass Properties Summary . . . . .	14



## List of Figures

1-1	Fatigue Stress Diagram for Steel . . . . .	2
1-2	Aeronca E-113 Crankshafts . . . . .	3
1-3	Failed E-113 Crankshaft . . . . .	4
1-4	Aeronca E-113 Airplane Engine as used in the C-3 Airplane . . . . .	4
1-5	Aeronca E-113 Engine Dynamic Components . . . . .	6
2-1	Location of propeller knife edge for moment of inertia measurement.	8
2-2	Location of crankshaft knife edge for moment of inertia measurement	9
2-3	Knife edge locations for connecting rod moment of inertia measurement . . . . .	9
2-4	Determination of connecting rod CG by suspending from two points.	10
2-5	Counterweight geometry for determining inertia properties . . . . .	11
2-6	Elemental shapes used to determine composite moment of inertia . . .	12
3-1	Ideal Otto Cycle compared with an actual cycle . . . . .	15
3-2	The indicator diagram developed from E-113 engine specifications. .	22
3-3	Cylinder volumes at point “a” and point “b” in the indicator diagram	22
3-4	Pressure profile of one complete engine cycle . . . . .	23
4-1	Definition of crank nomenclature . . . . .	25
4-2	Piston position, velocity, and acceleration at 2400RPM . . . . .	27
4-3	Graphical analysis of bench mark parameters . . . . .	27
4-4	Connecting rod kinematics including position, velocity, and acceleration . . . . .	31
4-5	Free body diagram of piston showing applied forces and accelerations . . . . .	33
4-6	Inertial forces on a piston at 2400RPM . . . . .	33
4-7	Free-body diagram of connecting rod with forces and accelerations . .	35
4-8	Crank pin inertial forces at 2400RPM . . . . .	36
4-9	Free-body diagram of crankshaft forces and accelerations . . . . .	39
4-10	Horizontal crankpin and counterweight forces . . . . .	39
4-11	Horizontal crankpin and counterweight forces with 1.5 times the Counterweight mass . . . . .	40
4-12	Crankshaft torque produced by a single cylinder . . . . .	41
4-13	Crankshaft torque from twin cylinder engine at 2400RPM with rated piston pressures . . . . .	43
4-14	Free-body diagram of crankshaft reacting loads from both cylinders .	44

4-15	Horizontal main bearing forces for twin cylinder engine at rated power and 2400RPM . . . . .	45
A-1	Manufacturer's performance Data . . . . .	55
B-1	Engine assembly cross-section showing internal components . . . . .	57
B-2	Engine rear view showing back case parts and internal components . . . . .	58
B-3	Crankshaft and connecting rod assembly . . . . .	59
B-4	Engine installation drawing showing overall dimensions . . . . .	60
C-1	Dynamic flight parameters which produce engine accelerations . . . . .	64
D-1	Piston inertial forces during rolling flight . . . . .	68
D-2	Piston inertial forces during yawing flight . . . . .	69
D-3	Piston inertial forces during pitching flight . . . . .	69
E-1	Zload_Parameters.m . . . . .	71
E-2	Zpiston_Kinematics.m . . . . .	72
E-3	Zrod_kinematics.m . . . . .	73
E-4	Zindicator.m . . . . .	74
E-5	Zpiston_inertia.m . . . . .	75
E-6	Zrod_inertia.m . . . . .	76
E-7	Zrod_forces.m . . . . .	77
E-8	Zcrank_forces.m . . . . .	78
E-9	Ztwin_torque.m . . . . .	79
E-10	Zmain_bearing_forces.m . . . . .	80
F-1	Aeronca E-113 airplane engine dynamic components including the pistons, connecting rods, and crankshaft shown with the propeller hub mounted . . . . .	82
F-2	Aeronca E-113 crankshaft assembly consisting of the forged crank, the main roller bearings, propeller hub and nut, and bolted on counterweights . . . . .	82
F-3	Back view of crankshaft assembly showing oil spindle hole, timing gear, main bearing, and counterweights . . . . .	83
F-4	Fixture for swinging the crankshaft assembly to determine the moment of inertia by supporting on knife edge through the crank pin lightening hole . . . . .	83
F-5	Forged connecting rod pair with bronze wrist pin bushings, split Babbitt crank pin bearing, and close tolerance clamp bolts/nuts . . . . .	84
F-6	Connecting rod shown suspended from knife edge for pendulum swing experiment . . . . .	85
F-7	Propeller knife edge inserted into a prop hub bolt hole . . . . .	85

## Nomenclature

A	Area
$A_X$	Piston acceleration
dM	Incremental mass
D	Diameter, dray
$F_G$	Gas force on piston
$F_H$	Horizontal main bearing force
$F_P$	Piston force
$F_S$	Vertical force on the piston pin
$F_V$	Vertical main bearing force
$F_W$	Cylinder wall reaction against piston
$F_X$	Horizontal crank pin force
$F_Y$	Vertical crank pin force
g	gravitational constant
$I_{CG}$	Moment of inertia about the center of gravity
I	Moment of inertia
$I_C$	Moment of inertia about crankshaft center of rotation
$I_{CW}$	Moment of inertia of counterweight
$I_o$	Moment of inertia about "O"
$I_P$	Moment of inertia of propeller
$I_R$	Moment of inertia of connecting rod about center of mass
$I_{RO}$	Moment of inertia of connecting rod about piston pin
$I_{XX}$	Moment of inertia on horizontal axis passing through center of mass
$I_{YY}$	Moment of inertia about vertical axis passing through center of mass
k	a constant
$K_{CW}$	Radius of gyration of the counterweight
L	Length of connecting rod
$L_1$	Location of connection rod center of mass from big end center
$L_2$	Location of connection rod center of mass from small end center
M	Mass
$M_P$	Mass of piston
$M_R$	Mass of connecting rod
$M_{CW}$	Mass of counterweight
N	Rotational speed
p	Pressure, roll rate

q	Pitch rate
r	radius, arm, compression ratio, yaw rate
R	Crank pin radius
S	Stroke
T	Engine torque, pendulum period, thrust
V	Volume, displacement, velocity
$V_x$	Piston velocity
W	Work, weight
x	Distance along the “x” coordinate axis
X	Piston position from crankshaft center to piston pin
$X_C$	Projection of crank arm on horizontal axis
$X_L$	Projection of connecting rod on horizontal axis
y	Distance along the “y” coordinate axis
$Y_C$	Projection of crank arm on vertical axis
$\alpha_a$	Crankshaft angular acceleration
$\alpha_b$	Connecting rod angular acceleration
$\omega_a$	Crankshaft angular velocity
$\omega_b$	Connecting rod angular velocity
$\Phi_a$	Crankshaft angle
$\theta_b$	Connecting rod angle
$\gamma$	Ratio of specific heats

## Acronyms

BDC	Bottom Dead Center
BMEP	Brake Mean Effective Pressure
CG	Center of Gravity
FAA	Federal Aviation Administration
FCC	Federal Communications Commission
IMEP	Indicated Mean Effective Pressure
MATLAB <sup>®</sup>	Matrix Laboratory
RPM	Revolutions per minute
S <sub>N</sub>	Stress versus number of load cycles
TBO	Time between overhauls
TDC	Top Dead Center

## 1.0 Introduction

In speaking of aircraft crankshafts, the subject of metal fatigue soon follows. Rarely does a crankshaft fail due to an overload, prop strikes excluded. It is more likely the relentless cycle of load reversals occurring over a long period of time that leads to a final catastrophic event. A fatigue failure starts with a minuscule crack. It is only through inspections, such as time-between-overhaul (TBO) inspections, that the opportunity to find these cracks can occur.

It is not unreasonable to expect an airplane engine crankshaft to last indefinitely. In studying the stress versus load cycles ( $S-N$ ) diagram for steel in figure 1-1, one can see that below a certain endurance stress level ( $S_e$ ) the metal will not crack no matter the number of load cycles. Good design practice would put stresses below that limit. However, the need to reduce weight by eliminating excess metal and the need to provide good fatigue resistance leads to conflicting objectives. A compromise is needed as well as an analytical method to model crankshaft loads.

Below in figure 1-2 are shown two styles of crankshaft used in the Aeronca E-113 airplane engine. Over a period of years, a number of changes were made to the design to counter a problematic history of fatigue failures.

Also shown below in figure 1-3 is an E-113 crankshaft that has already experienced a fatigue failure. Stress concentrations in the roots of the splines started a crack progression that gradually weakened the shaft until normal flight loads were sufficient to fracture the remaining metal. The remnants of a crack are still visible at a  $45^\circ$  angle over the top of the extension shaft. Such a  $45^\circ$  alignment is indicative of torsional loading.

With the advent of diesel engine aircraft, much higher combustion pressures will become a factor. Compression ratios on the order of 20:1 will require much stronger engine components yet weight concerns will remain. Advances in materials, manufacturing methods, and surface treatments will surely be required.

It is known that for the same power output, engine weight can be reduced by operating the engine at higher rotational speeds. However, the efficiency of the propeller suffers at higher speed. The incorporation of speed reduction units whether based on gear, belt, or chain becomes attractive. Again, the pulsating torque characteristic of a piston engine hinders building a survivable unit.

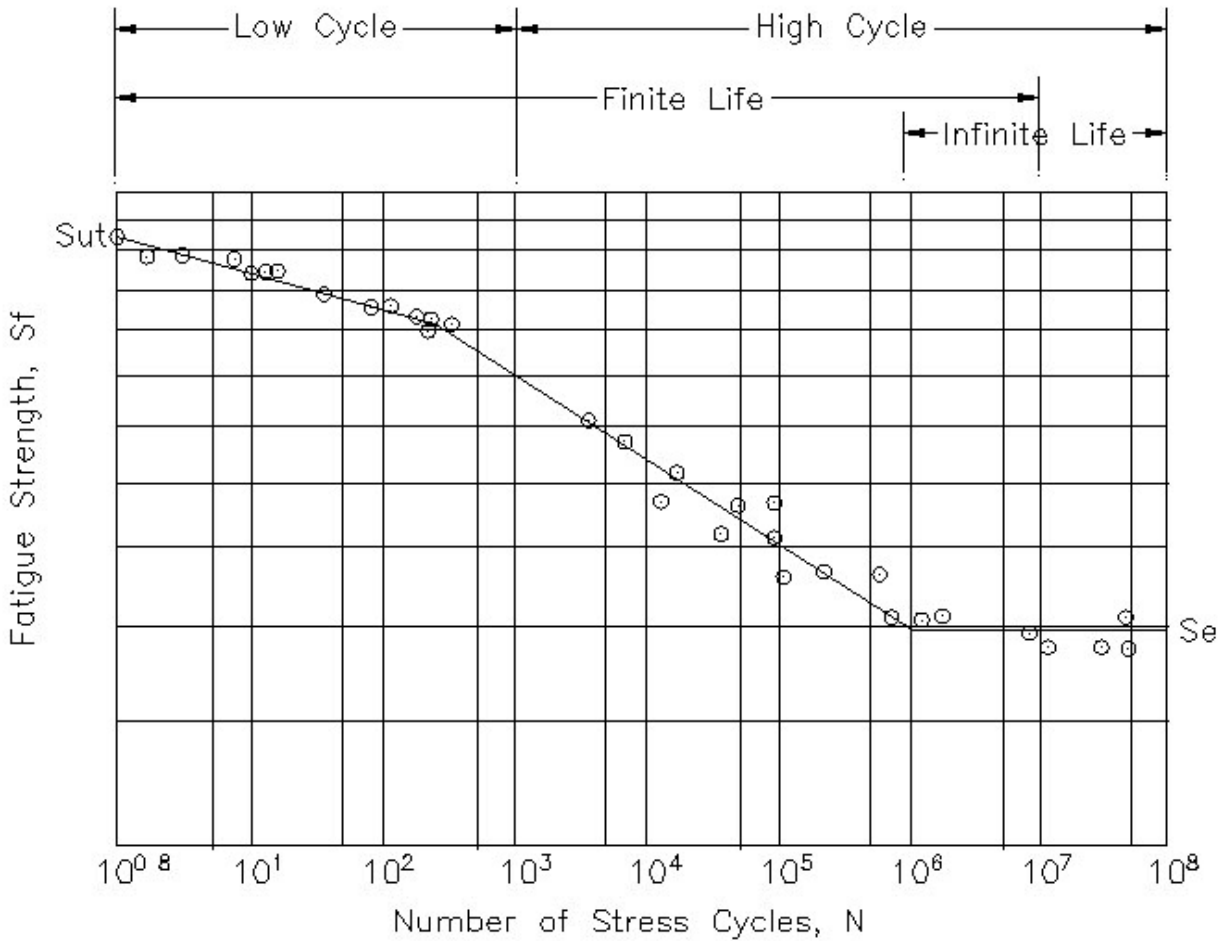


Figure 1-1 Fatigue Stress Diagram for Steel

Purpose built aircraft engines are designed, tested, manufactured, and supported in relatively small numbers as compared to the automotive market. As a result, a smaller number of units bear the entire cost to develop and to produce them. It is inviting to consider the use of a mass produced automotive engine in an aircraft. If all the concerns about quality control, high altitude capability, and continuous power rating could be resolved, the issue of crankshaft reliability remains, including the lack of a suitable thrust bearing and the ability to handle the propeller's inertial and gyroscopic loads.

It is the result of the above considerations that this study was embarked upon as a design tool for estimating crankshaft, as well as connecting rod and piston loads. A number of simplifying assumptions were made to make the analysis manageable yet err on the conservative side. These include the requirement that the members are rigid and do not oscillate elastically in the speed range being considered (no

flex). The crankcase has infinite mass (no shake), and the propeller looks like an infinite flywheel maintaining a constant angular velocity and torque reaction equal to the operating point of the actual propeller. Likewise, intentional omission is made of other dynamic components such as the camshaft, magneto, and oil pump which are clearly present in a functioning engine and provide additional inertia and load.

The basic element under consideration was a single cylinder power plant, having four operating strokes, balancing counterweights, and operating at sea level. Of course, any number of variations can be made by later changing equation parameters. Having developed relationships for a single cylinder, the analysis was expanded to a horizontally opposed, twin cylinder engine such as the Aeronca E-113 which was used as a case study.



Figure 1-2 Two styles of Aeronca E-113 Crankshafts





Figure 1-3 E-113 crankshaft failed due to fatigue at root of spines

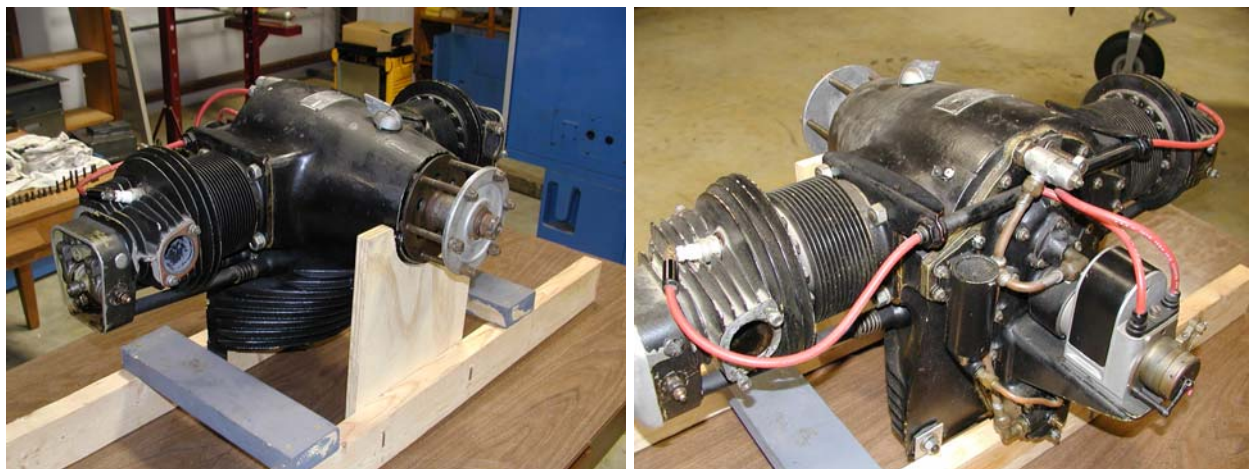


Figure 1-4 The Aeronca E-113 Airplane Engine as Used in the C-3 Airplane

# 1.1 The Aeronca E-113 Airplane Engine

This engine was used for several reasons: (1) it is typical of the current configuration of aircraft piston engines, (2) the engine is uncomplicated by modern performance enhancing accessories, and (3) loose engine components were available for measurement without having to disassemble a functioning engine. Figure 1-4 above shows views of an example engine. Some of the relevant specifications are shown in Table 1-1 below.

Figure 1-5 below shows the major dynamic components within the engine including the crankshaft assembly, the connecting rods, and pistons. See Appendix B for engine drawings.

TABLE 1-1 Aeronca E-113 Engine Specifications

Parameter	Value
Number of Cylinders	Two
Horsepower Rating	36HP at 2400RPM <sup>1</sup>
Cylinder Bore	4.25" diam.
Stroke	4.00"
Piston Displacement	113.5 in <sup>3</sup>
Compression Ratio	5.4:1
Connecting Rod Length	6.625"

Notes: 1. See Appendix A for dynamometer curves

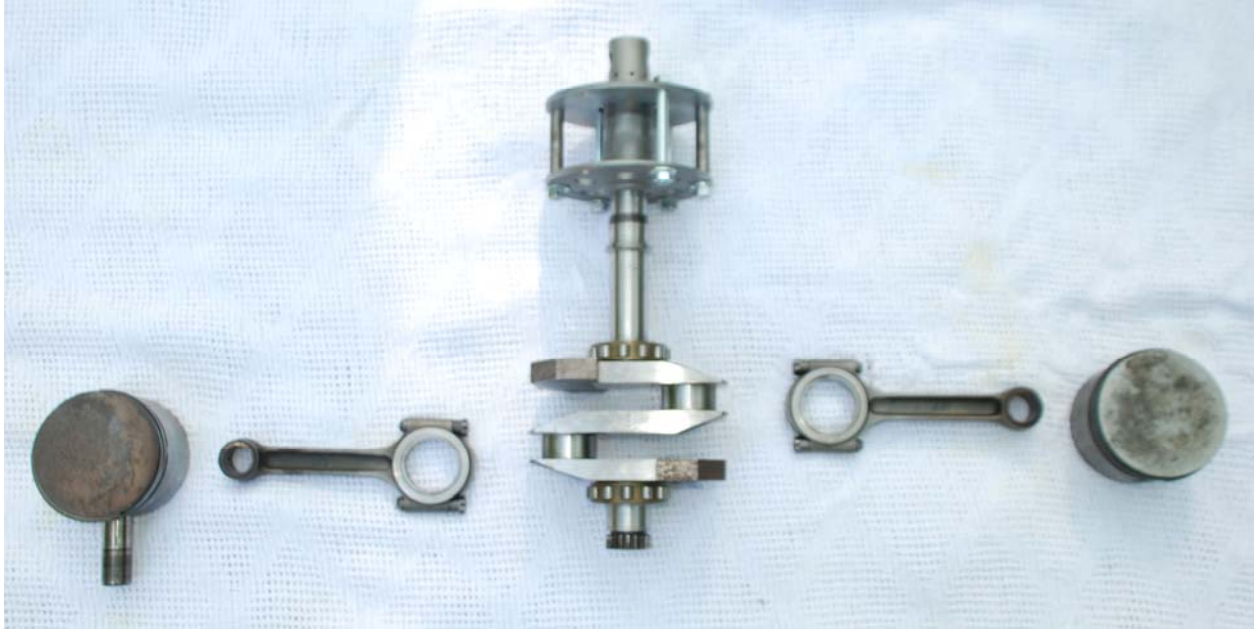


Figure 1-5 Aeronca E-113 Engine Dynamic Components

## 1.2 Software Tools

MATLAB<sup>®</sup> was the primary tool used to manipulate data and produce plots. Many equations were solved or at least verified using the “Symbolic Math” tool box. Appendix E provides a listing of the applicable scripts written for this effort.

## 2.0 Component Weights and Inertias

### 2.1 Moment of Inertia Calculation

The moment of inertia of the propeller, crankshaft, and connecting rod were found by the pendulum method as described in Martin [5]. The components were hung from a knife edge as shown in figure 2-1, figure 2-2, and figure 2-3 below. By giving the body a small displacement and counting the number of oscillations over a time interval, it was possible to determine the moment of inertia. The equation below gives the pendulum equation.

$$T = 2\pi \sqrt{\frac{I_o}{M \cdot g \cdot r}}$$

Solving for  $I_o$

$$I_o = M \cdot g \cdot r \left( \frac{T}{2\pi} \right)^2$$

Where

$I_o$  = Moment of inertia about pivot point

$T$  = Time for one oscillation

$M$  = Mass of body

$r$  = Distance between pivot point and the center of mass

$g$  = Acceleration of gravity

From the parallel axis theorem, the moment of inertia was then referred to the center of mass.

$$I_o = I_{CG} + M \cdot r^2$$

$$I_{CG} = I_o - M \cdot r^2$$

Where

$I_{CG}$  = moment of inertia about center of mass

Table 2-1 below shows the results of the mass and inertia measurements.

Table 2-1 Summary of Mass Characteristics of E-113 Engine Components

Item	Weight	Mass	Time	Cycles	Period	Arm	Moment.
units	lbs	slug	sec	count	sec	inch	Lb-ft-sec <sup>2</sup>
Propeller	11.0	0.342	50.5	20	2.525	2.313	0.329
Crankshaft <sup>1</sup>	15.8	0.491	12.3	20	0.615	2.527	0.0101
Conn Rod <sup>2</sup>	1.88	0.0583	20.5	25	0.820	5.000	0.00319
Conn Rod <sup>3</sup>	1.88	0.0583	18.95	25	0.758	3.060	0.00318
Counter wt	2.14	0.0665	-	-	-	2.613 <sup>4</sup>	0.0032
Piston	2.24	0.0695	-	-	-	-	-

- Notes: 1. with counterweights, 0.00695 without counterweights  
 2. Suspended from small end  
 3. Suspended from big end  
 4. Radius of gyration

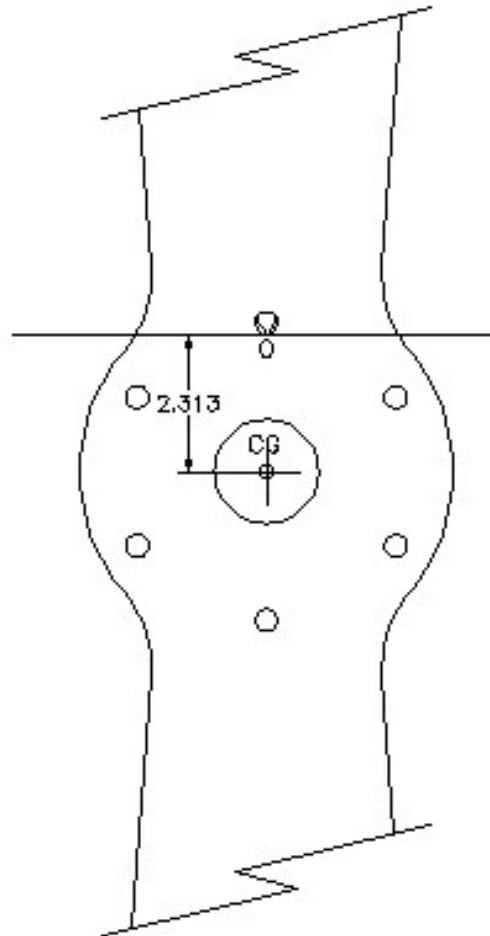


Figure 2-1 Location of propeller knife edge for moment of inertia measurement

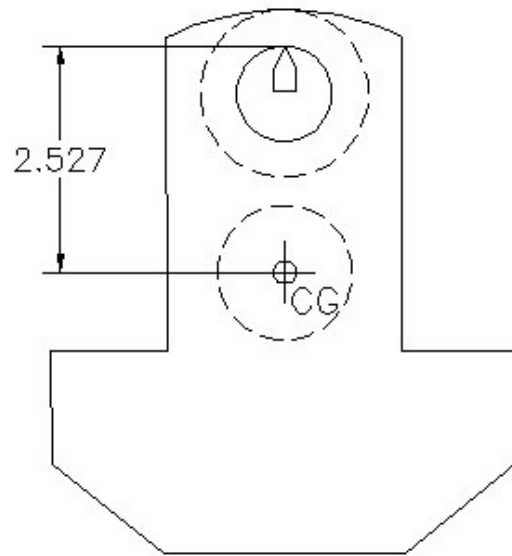


Figure 2-2 Location of crankshaft knife edge for moment of inertia measurement

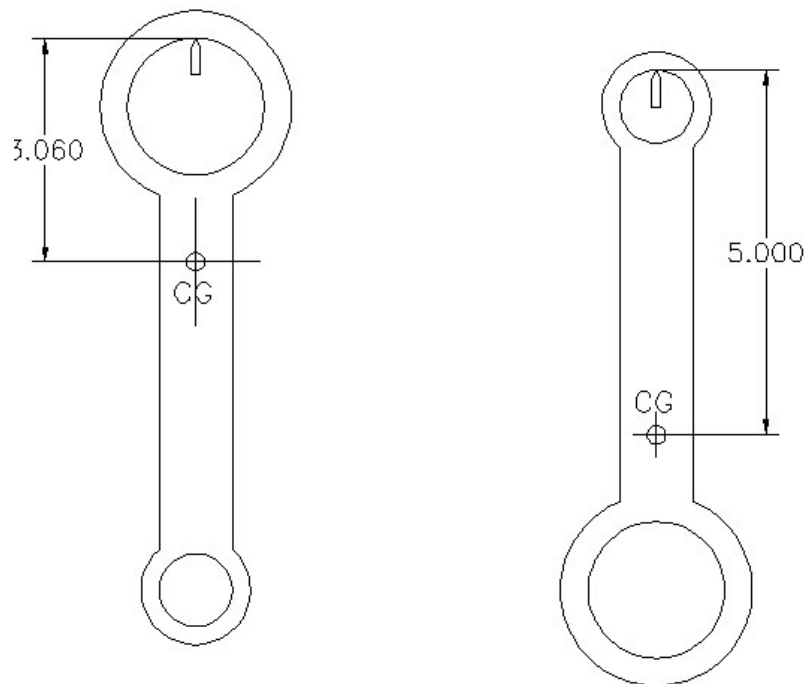


Figure 2-3 Knife edge locations for connecting rod moment of inertia Measurement

## 2.2 Connecting Rod Center of Gravity

An experiment was conducted to determine the center of gravity (CG) of the connecting rod as shown in figure 2-4. By alternately suspending the connecting rod by a string from two opposite clamp bolt heads, the vertical and center-to-center lines were projected and the resulting intersections were scaled. From the big end, measurements of 2.1160" and 2.2273" were found. The average of 2.1717" was used.



Figure 2-4 Determination of connecting rod CG by suspending from two points

## 2.3 Counterweight Mass and Inertia

The counterweights are bolted onto the E-113 crankshaft which leads to the intriguing possibility of removing and replacing them with different size weights for future dynamic balancing studies. However rather than actually disturbing the subject crankshaft, the mass properties of the counterweights were calculated and then deducted from the crankshaft assembly thereby itemized as separate components. Figure 2-5 below shows the shape and dimensions of a counterweight and how it is positioned with respect to the crankshaft journal, the center of rotation.

The moment of inertia can be computed in a general way by solving the equation below.

$$I = \int r^2 \cdot dM \quad \text{eq. (2-1)}$$

Considering the relatively complex shape, this equation would be cumbersome to solve. By representing the counterweight as a composite of elemental rectangles and triangles, the problem is more workable.

Figure 2-5 below shows how the counterweight has been divided into elemental shapes numbered 1 through 8. On each shape is indicated the center of gravity location about which the moment of inertia is required. Figure 2-6 below shows how the center of gravity is found on the rectangle and triangle.

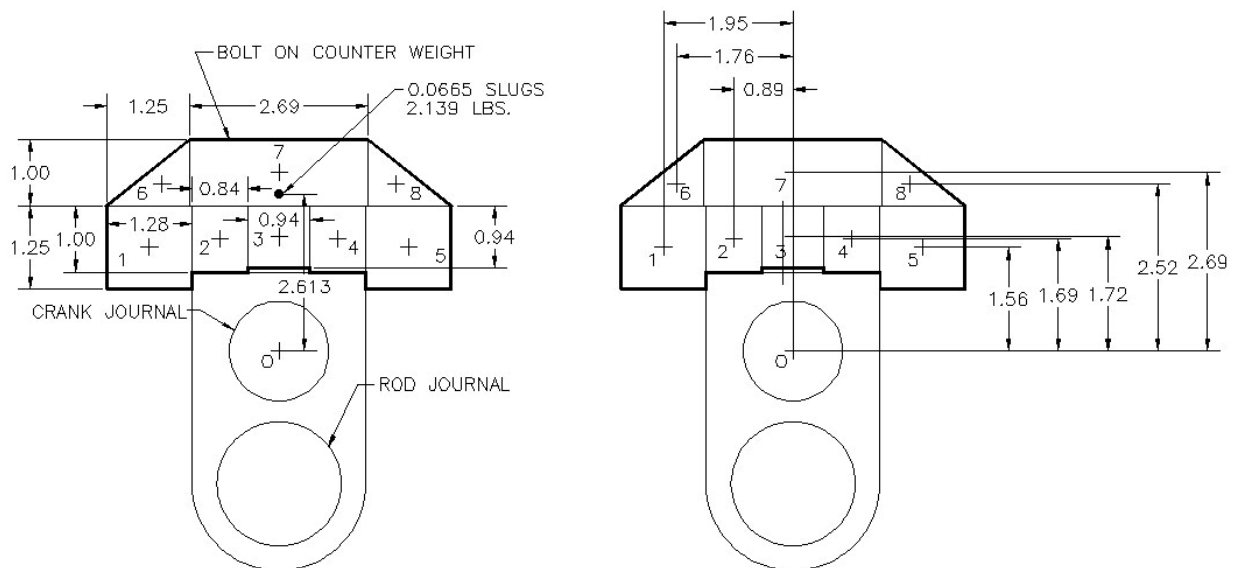


Figure 2-5 Counterweight geometry for determining inertial properties



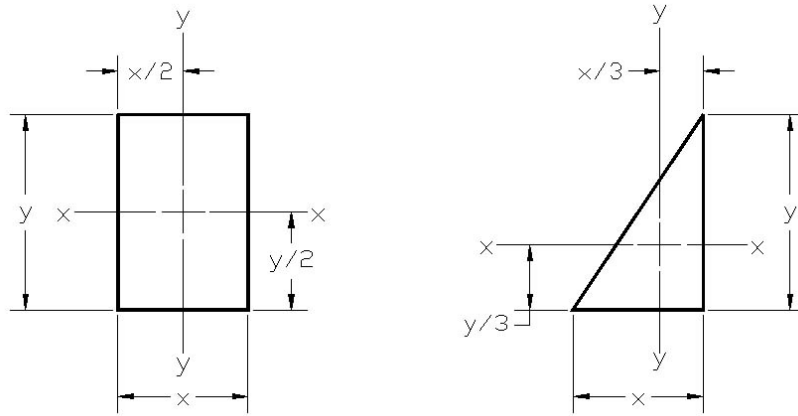


Figure 2-6 Elemental shapes used to determine composite moment of Inertia

Substitution into eq. (2-1) above,

$$r^2 = x^2 + y^2$$

$$I = \int (x^2 + y^2) \cdot dM$$

$$I = \int x^2 \cdot dM + \int y^2 \cdot dM$$

But  $I_{xx} = \int x^2 \cdot dM$  , and  $I_{yy} = \int y^2 \cdot dM$

Therefore  $I = I_{xx} + I_{yy}$  eq. (2-2)

Where  
 $I$  = Moment of Inertia of entire shape  
 $I_{xx}$  = Moment of Inertia about X-X axis  
 $I_{yy}$  = Moment of inertia about Y-Y axis  
 $dM$  = Mass increment

Moment of inertia “I”, as used above, is known as the polar moment of inertia and is simply the sum of the moments about the X-X and Y-Y axes.

For the rectangle,

$$I_{XX} = \frac{M \cdot y^2}{12}, \text{ and } I_{YY} = \frac{M \cdot x^2}{12}$$

Then 
$$I_{rect} = I_{XX} + I_{YY} = \frac{M}{12}(x^2 + y^2)$$

For the triangular,

$$I_{XX} = \frac{M \cdot y^2}{36}, \text{ and } I_{YY} = \frac{M \cdot x^2}{36}$$

Then 
$$I_{tri} = I_{XX} + I_{YY} = \frac{M}{36}(x^2 + y^2)$$

Where  $I_{rect}$  = Moment of inertia of rectangular shape  
 $I_{tri}$  = Moment of inertia of triangular shape  
 $M$  = Mass of solid three dimensional shape

The parallel axis theorem given below is then used to translate the moment of inertia to the crank axis

$$I_{CE} = I_E + r^2 M_E$$

Where  $I_{CE}$  = Moment of inertia of element referred to crank center of rotation  
 $I_E$  = Polar Moment of inertia of element  
 $M_E$  = Mass of element  
 $r$  = Distance from center of element mass to center of crank rotation

Based on the additional facts that the counterweight has a uniform thickness of 0.69” and the density of steel is 0.238 lb/in<sup>3</sup>, table 2-2 can be constructed below to find the polar moments, table 2-3 translates the moments to the crank journal, and table 2-4 gives the results.

Table 2-2 Counterweight mass characteristics

Segment	Height	Width	Depth	Mass	Polar Moment
	inch	inch	inch	slugs	Lb-ft-sec <sup>2</sup>
1	1.25	1.28	0.69	0.00971	1.7990E-05
2	1.00	0.84	0.69	0.00510	5.0327E-06
3	0.94	0.94	0.69	0.00536	5.4851E-06
4	1.00	0.84	0.69	0.00510	5.0327E-06
5	1.25	1.28	0.69	0.00971	1.7990E-05
6	1.00	1.25	0.69	0.00759	7.5011E-06
7	1.00	2.69	0.69	0.01633	7.7824E-05
8	1.00	1.25	0.69	0.00759	7.5011E-06

Table 2-3 Counterweight Moment Translation

Segment	Polar Moment	Distance r	Moment I <sub>C</sub>
	Lb-ft-sec <sup>2</sup>	inch	Lb-ft-sec <sup>2</sup>
1	1.7990E-05	2.500	0.00044
2	5.0327E-06	1.906	0.00013
3	5.4851E-06	1.716	0.00012
4	5.0327E-06	1.906	0.00013
5	1.7990E-05	2.500	0.00044
6	7.5011E-06	3.073	0.00050
7	7.7824E-05	2.685	0.00090
8	7.5011E-06	3.073	0.00050

Table 2-4 Counterweight Mass Properties Summary

Total Mass	Moment I <sub>C</sub>	Radius of Gyration
slug	Lb-ft-sec <sup>2</sup>	inch
0.06649	0.00315	2.61278

### 3.0 Piston Pressures

The Aeronca E-113 engine is a 4-stroke power plant having (1) compression, (2) combustion and expansion, (3) exhaust, and (4) induction strokes occurring over two revolutions of the crankshaft. Of the 4-strokes, it is only the expansion cycle following combustion that provides output power. The other strokes absorb power. The pressures developed in the engine cylinders can be modeled by the ideal Otto cycle as shown below in figure 3-1.

In a steam engine, the output power was determined by the pressures developed over the piston. Since an indicator measured the pressure, the type of diagram shown above became known as an “indicator diagram”. As can be seen, starting at point “a” the piston moves toward the combustion chamber compressing the fuel-air mixture. Near point “b” the spark plug fires, greatly increasing the heat and pressure in the cylinder causing point “c” to be reached at the same cylinder volume. The expanding gases force the piston down on the power stroke until point “d” is reached.

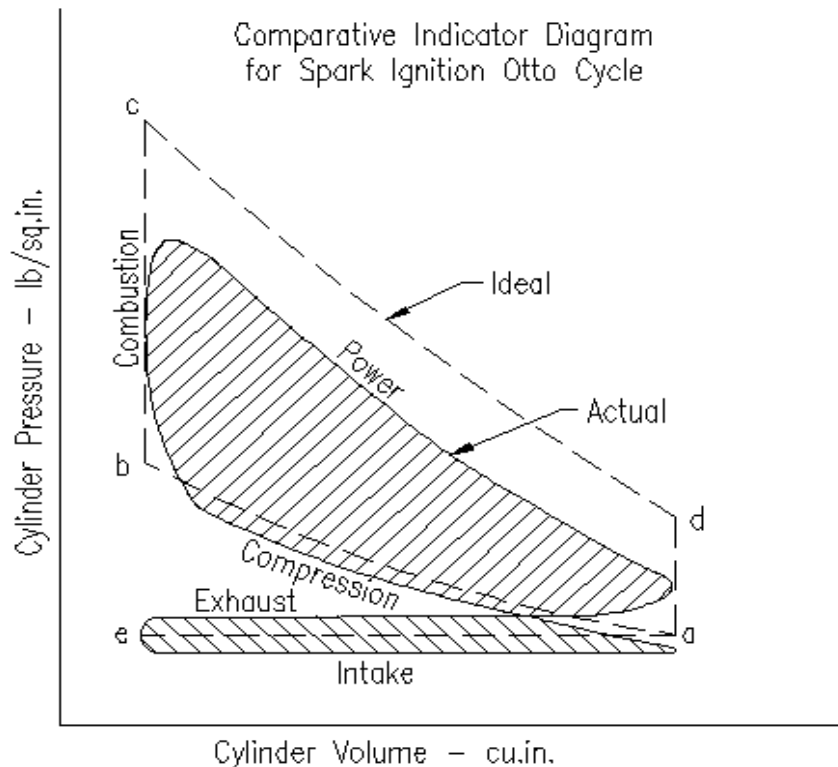


Figure 3-1 Ideal Otto Cycle compared with an actual cycle

The exhaust valve opens releasing the hot combustion products and the remaining pressure from the cylinder. For a 2-stroke engine, the cylinder state would return to point “a” and begin the next cycle. However, for the 4-stroke engine the exhaust valve opens and the piston pushes the gases out of the cylinder to point “e”. The exhaust valve closes and intake valve opens and a new fuel-air charge is drawn into the cylinder, returning to starting point “a”. This description, of course, ignores the practical need for spark advance, valve timing, and valve overlap which is dealt with the significant study of engine tuning.

For a proper analysis of the piston forces, it is necessary to consider the pressure measurements as being absolute pressures. Of course, a thorough analysis of piston forces would also consider crankcase pressures as acting on the underside of the piston. For simplicity, the crankcase is considered to be at atmospheric pressure since the large combustion pressures would well overshadow any error this might cause. In like manner, even though some work is required to move exhaust gases out and charge mixture in, this was lumped under the category of “pumping losses” in the following analysis.

As a further simplification, the relationship of cylinder pressures to volumes were modeled according to an isentropic process per Wark [39] where,

$$pV^\gamma = \text{Constant.}$$

Where:  $p$  = Absolute pressure  
 $V$  = Cylinder volume (including combustion chamber)  
 $\gamma$  = Ratio of specific heats

The value of  $\gamma$  above represents the ratio of specific heat  $c_p/c_v$  where  $c_p$  is the specific heat at constant pressure and  $c_v$  the specific heat at constant volume. The values chosen should match the mixture composition at working pressure and temperature. For a stoichiometric fuel-air mixture, Heywood [3] suggests a value of 1.3 for unburned charge and 1.2 for burned gas. Due to cooling of the exhaust mixture in real engines, the actual exhaust value may be higher, allowing a value of 1.3 to be a reasonable compromise for the entire cycle.

Since no indicator pressure data is actually available, it will be necessary to recreate such a diagram from known engine performance data. The brake mean effective pressure (BMEP) is a figure that describes the ability of an engine to

produce torque. By dividing the engine torque by the cylinder displacement and knowing that two engine revolutions are required for every torque producing cycle, a number having the units of pressure was determined.

$$BMEP = \frac{P \cdot b}{V \cdot N}$$

Where  $P$  = Engine power  
 $V$  = Displacement  
 $N$  = Rotational speed  
 $b$  = Revolutions per power stroke = 2 (for 4-stroke engine)

For the E-113 engine the following full throttle values apply:

$$BMEP = \frac{36HP \cdot \frac{33,000 \text{ ft} \cdot \text{lb.} / \text{min}}{HP} \cdot \frac{12 \text{ in}}{\text{ft}} \cdot \frac{2 \text{ rev}}{\text{powerstroke}}}{113.5 \text{ in}^3 \cdot 2400 \text{ rev} / \text{min}} = 104.7 \text{ lb} / \text{in}^2$$

The value so determined describes the pressure parameter at the output shaft of the engine where losses due to friction and pumping have taken place. The pressure value, if measured with a pressure transducer tapped into the combustion chamber (and averaged), would produce a higher value termed the indicated mean effective pressure (IMEP). It reflects more closely the pressures bearing on the piston. The BMEP is estimated to be between 80 to 90% of IMEP per Angle [1] and between 75 to 90% per Heywood [3]. The higher value is achieved at full throttle and moderate speed (1800 to 2400 RPM). The efficiency decreases when throttled or operated at high speed. By choosing a mid-value of 85%, an estimation of the IMEP can be made as follows:

$$IMEP = \frac{BMEP}{0.85} = \frac{104.7 \text{ lb} / \text{in}^2}{0.85} = 123.2 \text{ lb} / \text{in}^2$$

Returning to the indicator diagram, it can be seen that the area enclosed by the curves represents the work done on the piston by the gas pressures during the expansion stroke or done by the piston during compression. The pumping losses, already accounted, represent the exhaust and induction strokes. Now, by integrating the areas under the expansion and compression curves, subtracting, averaging, and equating to IMEP, the indicator diagram can be reproduced in

sufficient detail to characterize the pressures applied to the piston. The method described below follows that given by Angle [1].

$$W_{compression} = \int p \cdot dV$$

But: 
$$p = \frac{k}{V^\gamma}$$

Therefore: 
$$W_{compression} = \int_{V_b}^{V_a} \frac{k}{V^\gamma} \cdot dV = k \int_{V_b}^{V_a} V^{-\gamma} \cdot dV = \frac{k}{1-\gamma} [V^{1-\gamma}]_{V_b}^{V_a} = \frac{k}{1-\gamma} [V_a^{1-\gamma} - V_b^{1-\gamma}]$$

But: 
$$k = p_b V_b^\gamma$$

Therefore: 
$$W_{compression} = \frac{p_b V_b^\gamma}{1-\gamma} (V_a^{1-\gamma} - V_b^{1-\gamma}) = \frac{1}{1-\gamma} (p_b V_b^\gamma \cdot V_a^{1-\gamma} - p_b V_b^\gamma \cdot V_b^{1-\gamma})$$

But: 
$$p_a V_a^\gamma = p_b V_b^\gamma \quad \text{or} \quad V_b^\gamma = \frac{p_a}{p_b} V_a^\gamma$$

Therefore:

$$W_{compression} = \frac{1}{1-\gamma} \left( p_b \cdot \frac{p_a}{p_b} V_a^\gamma \cdot V_a^{1-\gamma} - p_b V_b \right) = \frac{p_a V_a - p_b V_b}{1-\gamma} = \frac{p_b V_b - p_a V_a}{\gamma-1}$$

Likewise: 
$$W_{expansion} = \frac{p_d V_d - p_c V_c}{1-\gamma} = \frac{p_c V_c - p_d V_d}{\gamma-1}$$

$$W_{expansion} - W_{compression} = \frac{(p_c V_c - p_d V_d) - (p_b V_b - p_a V_a)}{(\gamma-1)}$$

Averaging: 
$$\frac{(p_c V_c - p_d V_d) - (p_b V_b - p_a V_a)}{(V_a - V_b)(\gamma-1)} = IMEP \quad \text{eq. (3-1)}$$

Where:  $V_a$  = Volume at start of compression  
 $V_b$  = Volume at end of compression  
 $V_c$  = Volume at start of expansion  
 $V_d$  = Volume at end of expansion

$p_a$  = Pressure at start of compression

$p_b$  = Pressure at end of compression

$p_c$  = Pressure at start of expansion

$p_d$  = Pressure at end of expansion

To fully characterize the piston pressures, it will be necessary to establish a pressure and volume point on the compression and expansion curves, then use the relationship  $pV^\gamma = k$  to describe the remaining points. It can be assumed that the compression curve starts at point “a” near atmospheric pressure. A value of 13.0 psi rather than 14.7 psi is sometimes given per Heywood [3] to account for pressure loss in the induction system. The pressure at the end of the expansion stroke (point “d”) can then be found knowing:

$r = V_a / V_b = V_d / V_c =$  Compression ratio

$$V_a = V_d$$

$$V_b = V_c$$

$$V_a = V_d$$

$$V_a = V_b \cdot r$$

$$V_d = V_c \cdot r$$

$$V_a - V_b = V_b(r - 1)$$

$$p_b V_b^\gamma = p_a V_a^\gamma$$

$$p_c V_c^\gamma = p_d V_d^\gamma$$

$$p_b = p_a r^\gamma$$

$$p_c = p_d r^\gamma$$

Since 
$$IMEP = \frac{(p_c V_c - p_d V_d) - (p_b V_b - p_a V_a)}{(V_a - V_b)(\gamma - 1)} \quad \text{eq. (3-2)}$$

$$IMEP(V_a - V_b)(\gamma - 1) = p_c V_c - p_d V_d - p_b V_b + p_a V_a$$

$$p_d = \frac{-IMEP \cdot V_b(r - 1)(\gamma - 1)}{V_d} + \frac{p_c V_c}{V_d} - \frac{p_b V_b}{V_d} + \frac{p_a V_a}{V_d}$$

But  $V_a = V_d$ , and  $V_b = V_c$ , and  $\frac{V_a}{V_b} = r$ , and  $\frac{V_d}{V_c} = r$



Therefore 
$$p_d = \frac{-IMEP \cdot (r-1)(\gamma-1)}{r} + \frac{p_c}{r} - \frac{p_b}{r} + p_a$$

But: 
$$P_b = p_a r^\gamma \quad \text{and} \quad P_c = p_d r^\gamma$$

Therefore 
$$p_d - \frac{p_d r^\gamma}{r} = \frac{-IMEP \cdot (r-1)(\gamma-1)}{r} + p_a - \frac{p_a r^\gamma}{r}$$

$$p_d(r - r^\gamma) = -IMEP \cdot (r-1)(\gamma-1) + p_a(r - r^\gamma)$$

$$p_d = \frac{IMEP \cdot (r-1)(\gamma-1)}{(r^\gamma - r)} + p_a \quad \text{eq. (3-3)}$$

Now it will be possible to determine the end pressure on the expansion curve. Using the parameters for the E-113 engine, the following values can be substituted into eq. (3-3):

$$p_d = \frac{123.2 \text{ lb/in}^2 \cdot (5.4-1)(1.3-1)}{(5.4^{1.3} - 5.4)} + 13.0 \text{ lb/in}^2 = 58.7 \text{ lb/in}^2$$

Now it is possible to describe the compression and expansion curves knowing both end points as follows:

Since: 
$$p_{\text{expansion}} \cdot V_{\text{expansion}}^\gamma = p_d \cdot V_d^\gamma$$

$$p_{\text{expansion}} = p_d \left( \frac{V_d}{V_{\text{expansion}}} \right)^\gamma = (58.7 \text{ lb/in}^2) \left( \frac{139.3 \text{ in}^3}{V_{\text{expansion}}} \right)^{1.3}$$

And: 
$$p_{\text{compression}} = p_a \left( \frac{V_a}{V_{\text{compression}}} \right)^\gamma = (13.0 \text{ lb/in}^2) \left( \frac{139.3 \text{ in}^3}{V_{\text{compression}}} \right)^{1.3}$$

Figure 3-2 below, shows the indicator diagram resulting from the above computations. As can be seen, the compression stroke starts at “a” and proceeds to “b”. The spark occurs causing the pressure to increase to “c”, after which time the piston is forced down and the gases expand to point “d” where the exhaust valve opens and expels the hot combustion products.

As a check, the work performed around the loop was found by numerical integration and that value was divided by the cylinder displacement resulting in a figure of  $123.3 \cdot \text{lb}/\text{in}^2$ . The IMEP was determined to be  $123.2 \cdot \text{lb}/\text{in}^2$  in the above premise, indicating that the equations are correct in modeling the piston pressures.

In considering the volumes indicated above, it is necessary to know the engine volumes relating to point “a” (or “d”) and point “b” (or “c”). Point “b” reflects the total engine combustion chamber volume, and point “a” reflects the total combustion chamber and volume swept by the pistons. The following engine specifications are useful in making these determinations:

$$D_{cyl} = \text{Cylinder Diameter, } 4.25''$$

$$S = \text{Piston Stroke, } 4.00''$$

$$r = \text{Compression Ratio, } 5.4$$

As a result: 
$$A_{piston} = \pi \left( \frac{D_{cyl}}{2} \right)^2 = \pi \left( \frac{4.25}{2} \right)^2 = 14.186 \cdot \text{in}^2$$

$$V_{cylinder} = A_{piston} \cdot S = (14.186 \cdot \text{in}^2)(4.00) = 56.745 \cdot \text{in}^3$$

The value indicated above represents only one cylinder, whereas the assumption in relating IMEP to cylinder pressure was based on the full engine with two cylinders operating.

$$V_{engine} = (56.745 \cdot \text{in}^3 / \text{cyl.}) \cdot 2\text{cyl.} = 113.490 \cdot \text{in}^3$$

$$\frac{1}{r} = \frac{V_{chamber}}{V_{chamber} + V_{swept}}$$

$$V_{chamber} = \frac{V_{swept}}{(r-1)} = \frac{113.490 \cdot \text{in}^3}{(5.4-1)} = 25.793 \cdot \text{in}^3$$

Therefore  $V_b = V_c = 25.793 \cdot \text{in}^3$ , or  $12.897 \text{ in}^3$  per cylinder

$V_a = V_d = 25.793 \cdot \text{in}^3 + 113.490 \cdot \text{in}^3 = 139.283 \cdot \text{in}^3$ , or  $69.642 \text{ in}^3$  per cylinder

The figure 3-3 below shows the volumes depicted for one engine cylinder.

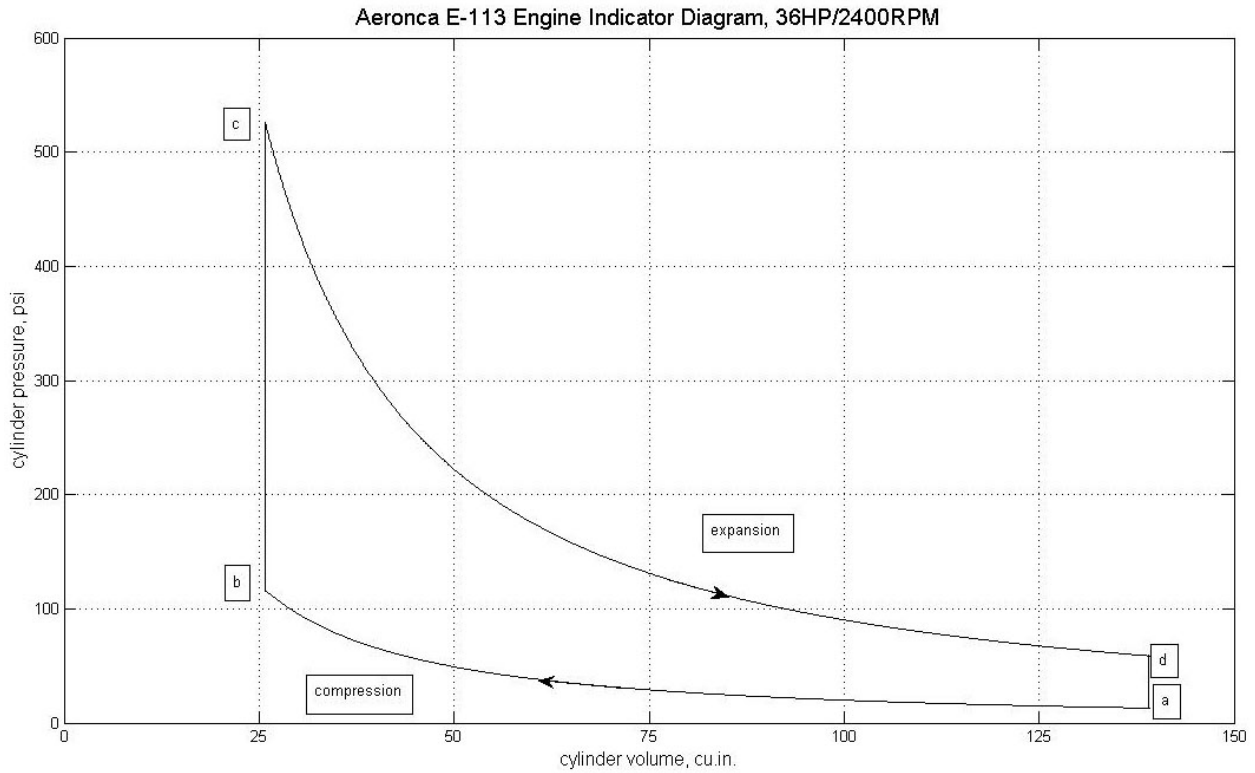


**Figure 3-2 The indicator diagram developed from E-113 engine specifications**

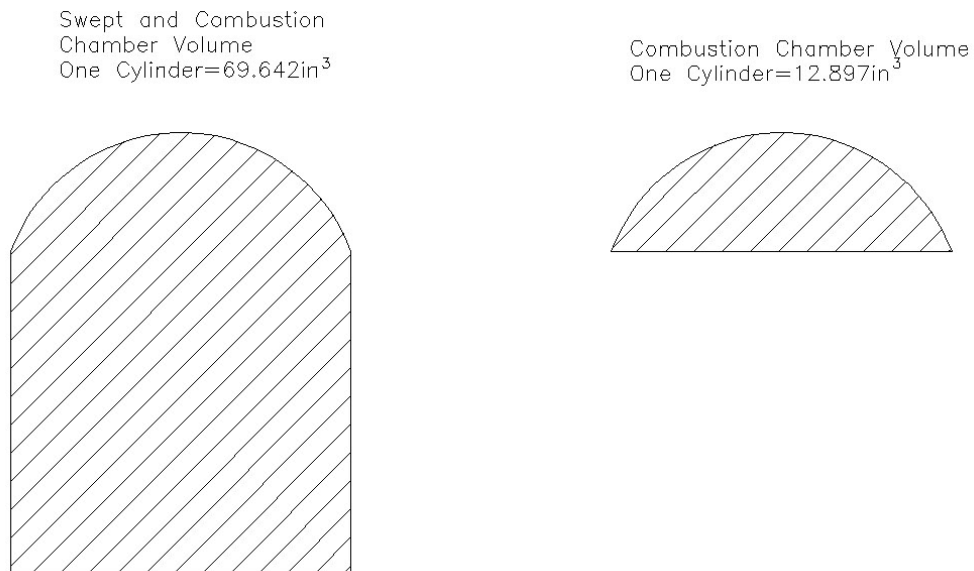


**Figure 3-3 Cylinder volume representation at point “a” and point “b” in the indicator diagram**

Figure 3-4 below gives a pressure profile for a complete engine cycle (4-strokes) including: intake, compression, expansion, and exhaust. The pressures have been converted to “gage” pressures by subtracting atmospheric pressure from the previously determined “absolute” cylinder pressures. This has been done since it is assumed that the crankcase will reside at atmospheric pressure and therefore gage pressure will reflect the pressure acting on the piston. Also, the absolute intake pressure was considered as 13.0 psia to account for losses in the induction system. Likewise, the absolute exhaust pressure was considered to be 15.5 psia to account for back pressure in the exhaust pipes. In spite of the addition of induction and exhaust “pumping” losses, on the scale of the plot, the effect is small. As can be seen, when the exhaust valve opens, a considerable loss in potential energy goes out the exhaust pipe, which subsequently led to the development of turbo-charging.

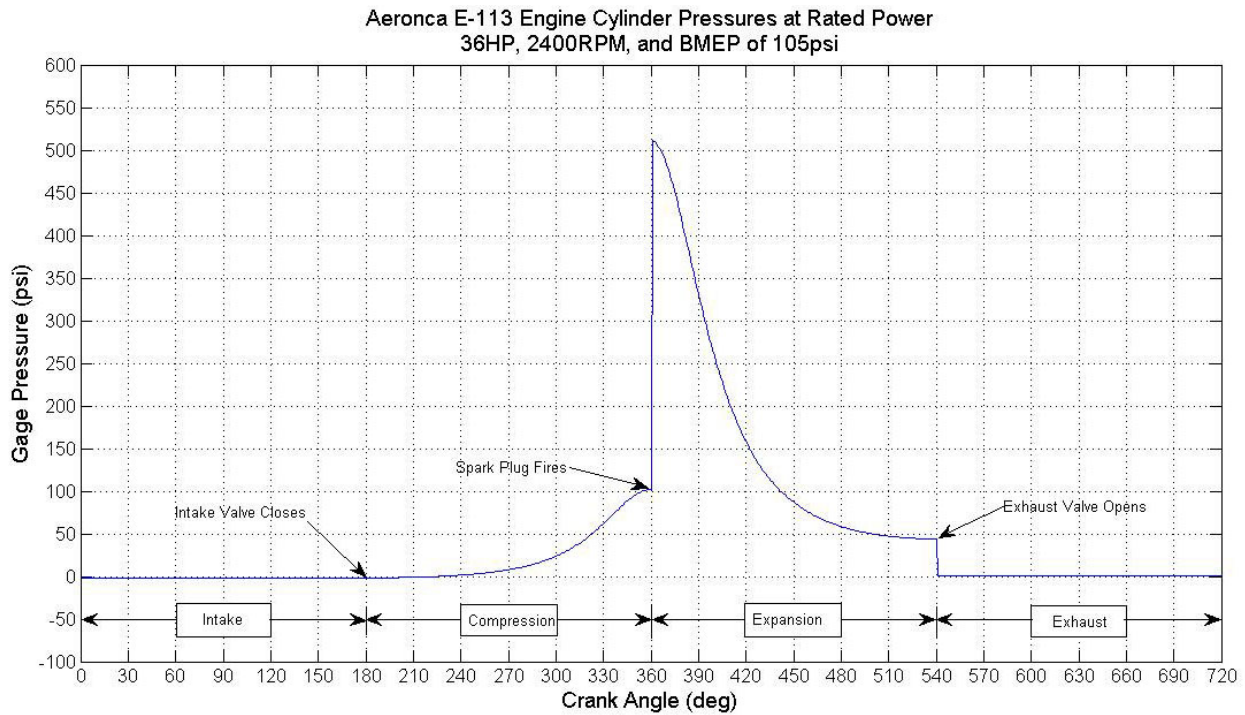


Figure 3-4 Pressure profile of one complete engine cycle

## 4.0 Crank Geometry and Kinematics

### 4.1 Piston Kinematics

Figure 4-1 below shows the symbols used to analyze the motions of the piston, connecting rod, and crankshaft. The crankshaft, shown on the left, rotates in a counterclockwise sense. The angular position, rate, and acceleration are given by  $\Phi_a$ ,  $\omega_a$ , and  $\alpha_a$  respectively. The crank radius is given by  $R$  (2.00"). The "top dead center" (TDC) crankshaft location is referred to as 0 radians ( $0^\circ$ ). Similarly, the "bottom dead center" (BDC) location is at  $\pi$  radians ( $180^\circ$ ). Two complete crankshaft revolutions comprise the 4-stroke engine cycle, extending from 0 to  $4\pi$  radians ( $0^\circ$  to  $720^\circ$ ). The projections of the crank arm onto the x and y axes are given by  $X_c$  and  $Y_c$ . A counterweight of mass  $M_{cw}$  (0.0665 slugs) is concentrated at a radius of gyration  $K_{cw}$  (2.613") from the crankshaft's center of rotation. The crankshaft has a rotational inertia of  $I_c$  (0.00695 lb-ft-sec<sup>2</sup>) about the crankshaft's center of rotation which is also its center of mass since the actual crankshaft is symmetrical about the two cylinders (one cylinder shown).

Considering the connecting rod, the angular position, rate, and acceleration are given by  $\theta_b$ ,  $\omega_b$ , and  $\alpha_b$ , respectively. The length of the connecting rod is given by  $L$  (6.625") and the center of mass,  $M_R$  (0.0583 slugs), is located  $L_1$  (2.17") and  $L_2$  (4.45") from the ends of the connecting rod. The rotational inertia of the connecting rod is  $I_R$  (0.00318 lb-ft-sec<sup>2</sup>) at its center of mass, and (0.0112 lb-ft-sec<sup>2</sup>) about the piston pin.

The piston has a mass  $M_p$  (0.0695 slugs), and experiences a linear velocity,  $V_x = dx/dt$ , and a linear acceleration,  $A_x = dV_x/dt = d^2x/dt^2$ . More discussion about piston velocity and acceleration will follow.

The piston pin position is established from an origin located at the center of crankshaft rotation. As can be seen from figure 4-1,

$$\text{Piston position} = x(\phi_a) = X_c + X_L$$

$$\text{But} \quad X_c = R \cdot \cos \phi_a, \quad \text{and} \quad Y_c = R \cdot \sin \phi_a$$

$$\text{And} \quad L^2 = Y_c^2 + X_L^2, \quad \text{therefore,} \quad X_L = \sqrt{L^2 - (R \cdot \sin \phi_a)^2}$$

Therefore: 
$$x(\phi_a) = R \cdot \cos \phi_a + \sqrt{L^2 - (R \cdot \sin \phi_a)^2}$$
 eq. (4-1)

To find the piston velocity, the above equation for  $x(\phi_a)$  will be differentiated with respect to crankshaft angle  $\Phi_a$  and thereafter transformed into a function of time.

$$\frac{dx}{d\phi_a} = -R \cdot \sin \phi_a + \frac{1}{2} [L^2 - (R \cdot \sin \phi_a)^2]^{\frac{1}{2}} \cdot (-2)(R \cdot \sin \phi_a)(R \cdot \cos \phi_a)$$

$$\frac{dx}{d\phi_a} = -R \cdot \sin \phi_a - \frac{R^2 (\sin \phi_a)(\cos \phi_a)}{\sqrt{L^2 - (R \cdot \sin \phi_a)^2}}$$

Since 
$$\frac{dx}{dt} = \frac{dx}{d\phi_a} \cdot \frac{d\phi_a}{dt}, \quad \text{and} \quad \frac{d\phi_a}{dt} = \omega_a$$

Then 
$$V_x = \frac{dx}{dt} = \left[ -R \cdot \sin \phi_a - \frac{R^2 (\sin \phi_a)(\cos \phi_a)}{\sqrt{L^2 - (R \cdot \sin \phi_a)^2}} \right] \cdot \omega_a$$
 eq. (4-2)

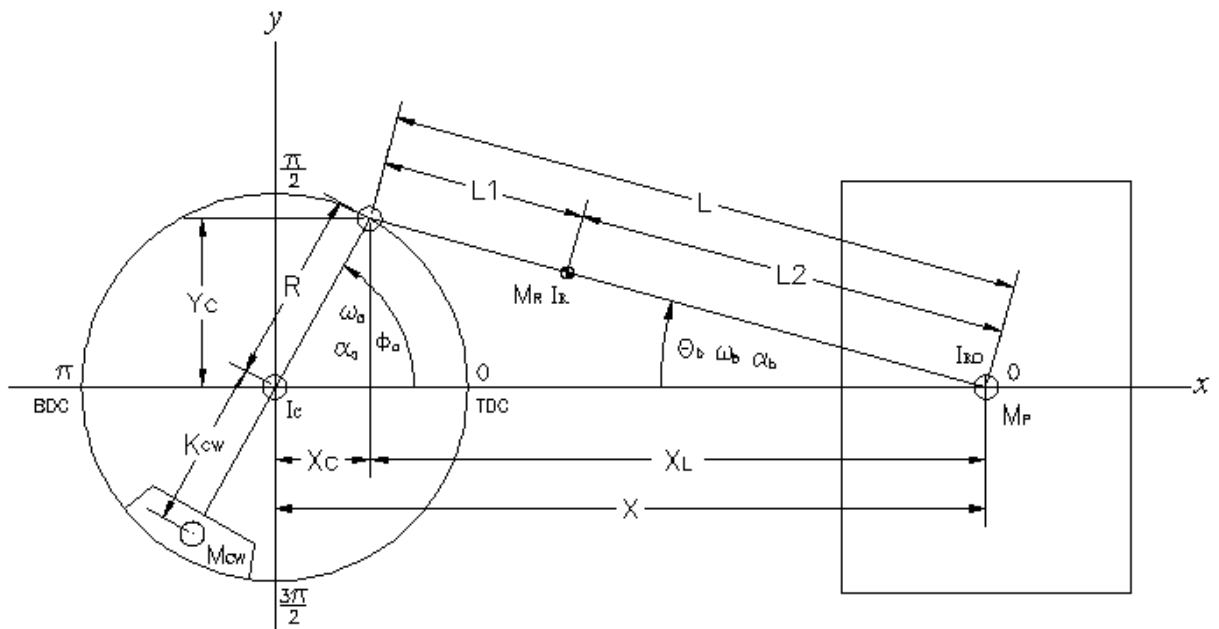


Figure 4-1 Definition of crank nomenclature

In like manner, the piston acceleration can be found by taking the second differential of  $x$  with respect to crankshaft angle.

$$\frac{d^2x}{d\phi_a^2} = -R \cdot \cos\phi_a + \frac{R^2(\sin^2\phi_a - \cos^2\phi_a)}{\sqrt{L^2 - (R \cdot \sin\phi_a)^2}} - \frac{R^4(\sin^2\phi_a)(\cos^2\phi_a)}{\left[\sqrt{L^2 - (R \cdot \sin\phi_a)^2}\right]^3}$$

Since 
$$\frac{d^2x}{dt^2} = \frac{d}{dt} \left( \frac{dx}{dt} \right) = \frac{d}{dt} \left( \frac{dx}{d\phi_a} \cdot \frac{d\phi_a}{dt} \right)$$

Further 
$$\frac{d^2x}{dt^2} = \frac{d}{dt} \left( \frac{dx}{d\phi_a} \right) \cdot \frac{d\phi_a}{dt} + \frac{dx}{d\phi_a} \cdot \frac{d^2\phi_a}{dt^2}$$

Therefore 
$$\frac{d^2x}{dt^2} = \frac{d^2x}{d\phi_a^2} \cdot \left( \frac{d\phi_a}{dt} \right)^2 + \frac{dx}{d\phi_a} \cdot \left( \frac{d^2\phi_a}{dt^2} \right)$$

But 
$$\left( \frac{d\phi_a}{dt} \right)^2 = \omega_a^2, \quad \text{and} \quad \left( \frac{d^2\phi_a}{dt^2} \right) = \alpha_a$$

Therefore 
$$A_x = \frac{d^2x}{dt^2} = \left[ -R \cdot \cos\phi_a + \frac{R^2(\sin^2\phi_a - \cos^2\phi_a)}{\sqrt{L^2 - (R \cdot \sin\phi_a)^2}} - \frac{R^4(\sin^2\phi_a)(\cos^2\phi_a)}{\left[\sqrt{L^2 - (R \cdot \sin\phi_a)^2}\right]^3} \right] \cdot \omega_a^2 + \left[ -R \cdot \sin\phi_a - \frac{R^2(\sin\phi_a)(\cos\phi_a)}{\sqrt{L^2 - (R \cdot \sin\phi_a)^2}} \right] \cdot \alpha_a \quad \text{eq. (4-3)}$$

Based on the above equations, Figure 4-2 below plots piston position, velocity, and acceleration when the engine is turning at 2400RPM. The piston position is referenced from the center of crankshaft rotation to the piston pin. The velocity and acceleration are positive in the direction of the cylinder head.

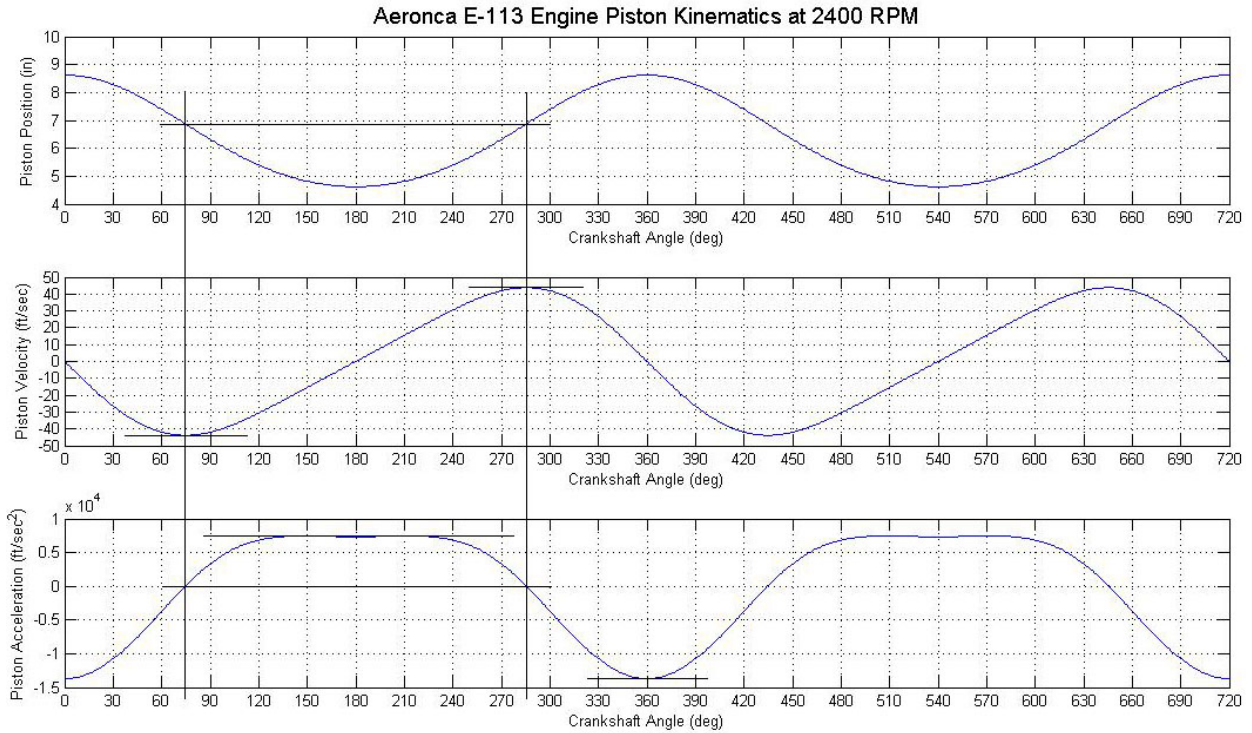


Figure 4-2 Piston position, velocity, and acceleration at 2400 RPM

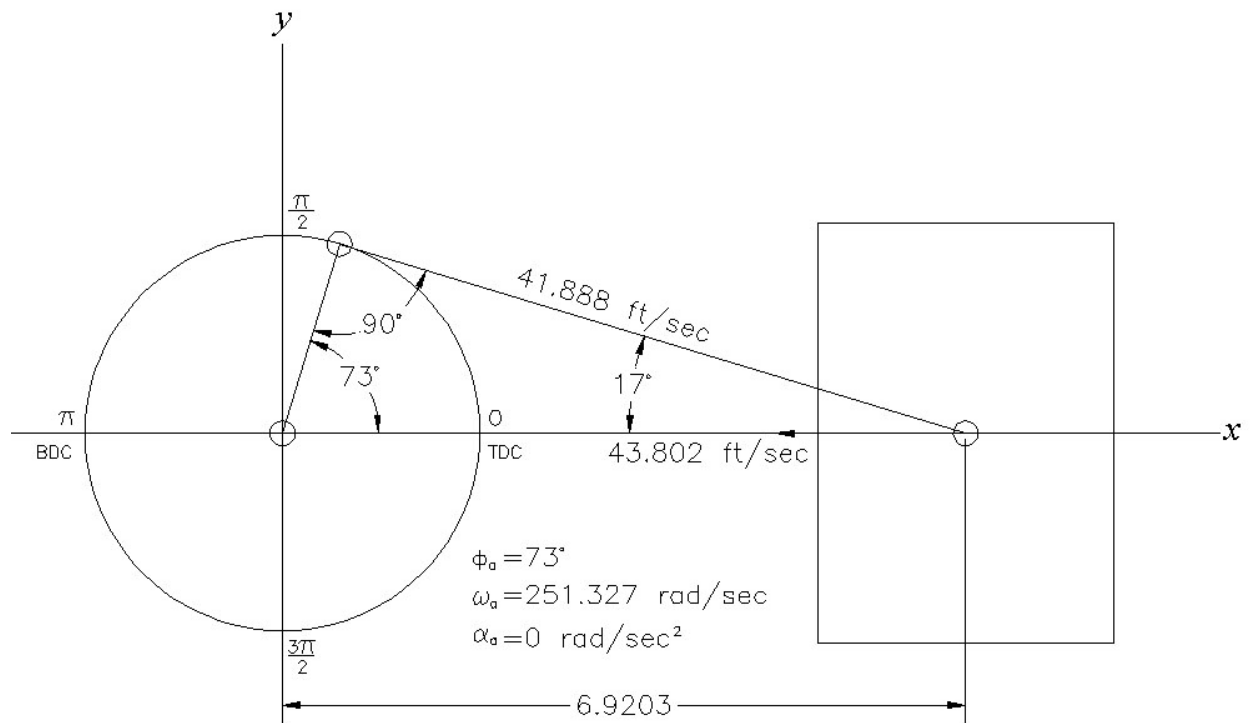


Figure 4-3 Analysis of geometry at maximum piston speed



It can be seen, the piston velocity is zero at either TDC or BDC. Of course, these are locations where the piston momentarily stops and changes direction. From the analysis done above in figure 4-3, it can be seen that the piston acceleration is zero when the piston position is 6.92 inches, velocity is a maximum at 43.8 ft/sec, and when the crankshaft is near the  $73^\circ$  and  $287^\circ$  positions. This can be verified with the kinematic plots in figure 4-2 above.

## 4-2 Connecting Rod Kinematics

Reference is made to figure 4-1 repeated below for the following discussion. As can be seen, when the crankshaft first turns counterclockwise, the connecting rod rotates clockwise until the crankshaft passes the 90° point, then they both rotate counterclockwise. When the crankshaft passes the 270° point they again rotate in opposite directions.

The connecting rod angle can be determined as follows.

$$\sin \theta_b = \frac{Y_C}{L}$$

But  $Y_C = R \cdot \sin \phi_a$ , and  $\sin \theta_b = \frac{R \cdot \sin \phi_a}{L}$

Therefore  $\theta_b = \arcsin\left(\frac{R}{L} \cdot \sin \phi_a\right)$  eq. (4-4)

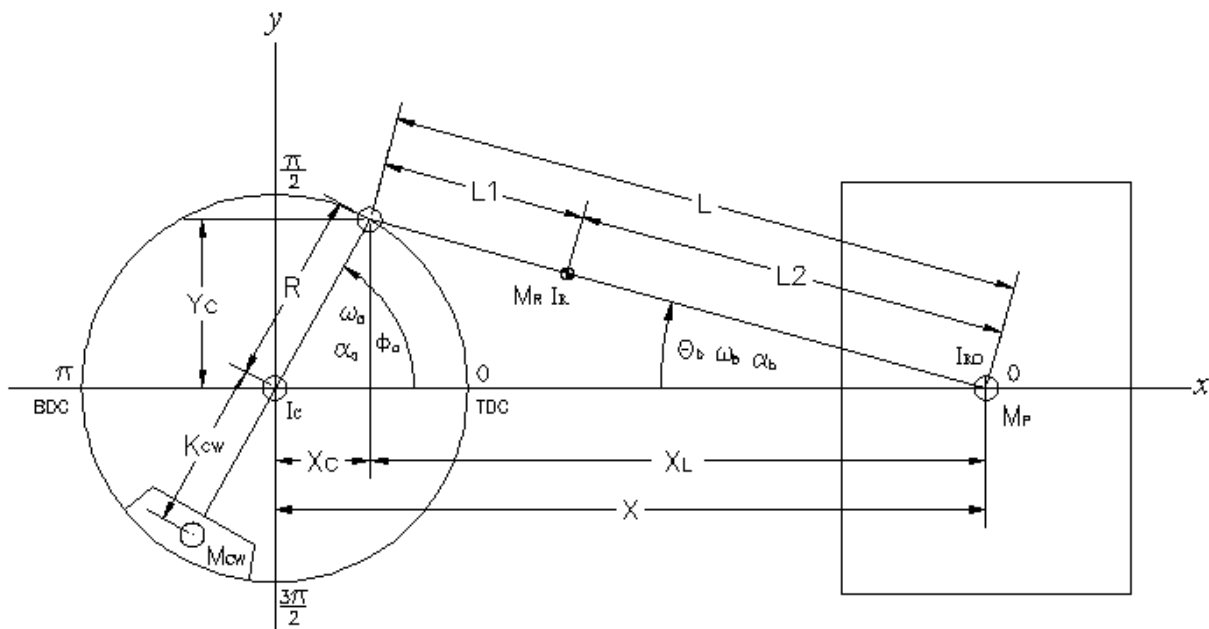


Figure 4-1 Definition of crank nomenclature repeated from above

By taking the first derivative of connecting rod angle, the connecting rod angular rate can be determined. Note that the derivative of the arcsine has the form,

$$\frac{d}{dx}(\arcsin u) = \frac{1}{\sqrt{1-u^2}} \cdot \frac{du}{dx}$$

Where  $u = \frac{R}{L} \cdot \sin \phi_a$ , and  $x = \phi_a$

Therefore 
$$\frac{d\theta_b}{d\phi_a} = \frac{1}{\sqrt{1-\left(\frac{R}{L}\sin\phi_a\right)^2}} \cdot \frac{R}{L}\cos\phi_a$$

Where 
$$\frac{du}{d\phi_a} = \frac{R}{L}\cos\phi_a$$

But 
$$\frac{d\theta_b}{dt} = \frac{d\theta_b}{d\phi_a} \cdot \frac{d\phi_a}{dt}, \text{ and } \frac{d\phi_a}{dt} = \omega_a$$

Therefore 
$$\omega_b = \frac{d\theta_b}{dt} = \frac{R \cdot \cos \phi_a}{\sqrt{L^2 - (R \cdot \sin \phi_a)^2}} \cdot \omega_a \quad \text{eq. (4-5)}$$

Where  $\omega_b =$  connecting rod angular velocity

Likewise, the angular acceleration can be found by taking the second derivative of the angular position.

$$\frac{d^2\theta_b}{d\phi_a^2} = -\frac{R \cdot \sin \phi_a}{\sqrt{L^2 - (R \cdot \sin \phi_a)^2}} + \frac{R^3 \cdot \sin \phi_a (\cos \phi_a)^2}{\left[\sqrt{L^2 - (R \cdot \sin \phi_a)^2}\right]^3}$$

But 
$$\frac{d^2\theta_b}{dt^2} = \frac{d^2\theta_b}{d\phi_a^2} \cdot \left(\frac{d\phi_a}{dt}\right)^2 + \frac{d\theta_b}{d\phi_a} \cdot \left(\frac{d^2\phi_a}{dt^2}\right),$$

and 
$$\frac{d\phi_a}{dt} = \omega_a, \text{ and } \frac{d^2\phi_a}{dt^2} = \alpha_a$$

Therefore,

$$\alpha_b = \frac{d^2\theta_b}{dt^2} = \left[ -\frac{R \cdot \sin \phi_a}{\sqrt{L^2 - (R \cdot \sin \phi_a)^2}} + \frac{R^3 \cdot \sin \phi_a (\cos \phi_a)^2}{\left[ \sqrt{L^2 - (R \cdot \sin \phi_a)^2} \right]^3} \right] \cdot \omega_a^2 + \left[ \frac{R \cdot \cos \phi_a}{\sqrt{L^2 - (R \cdot \sin \phi_a)^2}} \right] \cdot \alpha_a$$

eq. (4-6)

Where  $\alpha_b$  = connecting rod angular acceleration

Figure 4-4 below shows a plot of the above relationships over two revolutions of the crankshaft. The top plot shows the connecting rod angle (in degrees) with the zero degree position in line with the cylinder axis. Positive angles, velocities, and accelerations correspond to the conventions given in Figure 4-1 above. As can be seen, the connecting rod angular velocity (in rad/sec) is greatest at 0°, 180°, and multiples thereof because the crank pin is traveling at right angles to the cylinder axis. Connecting rod angular velocity is a minimum at 90°, 270°, and so on since the crank pin is moving parallel to the cylinder axis. As expected, the position, velocity, and acceleration responses are displaced 90° from each other.

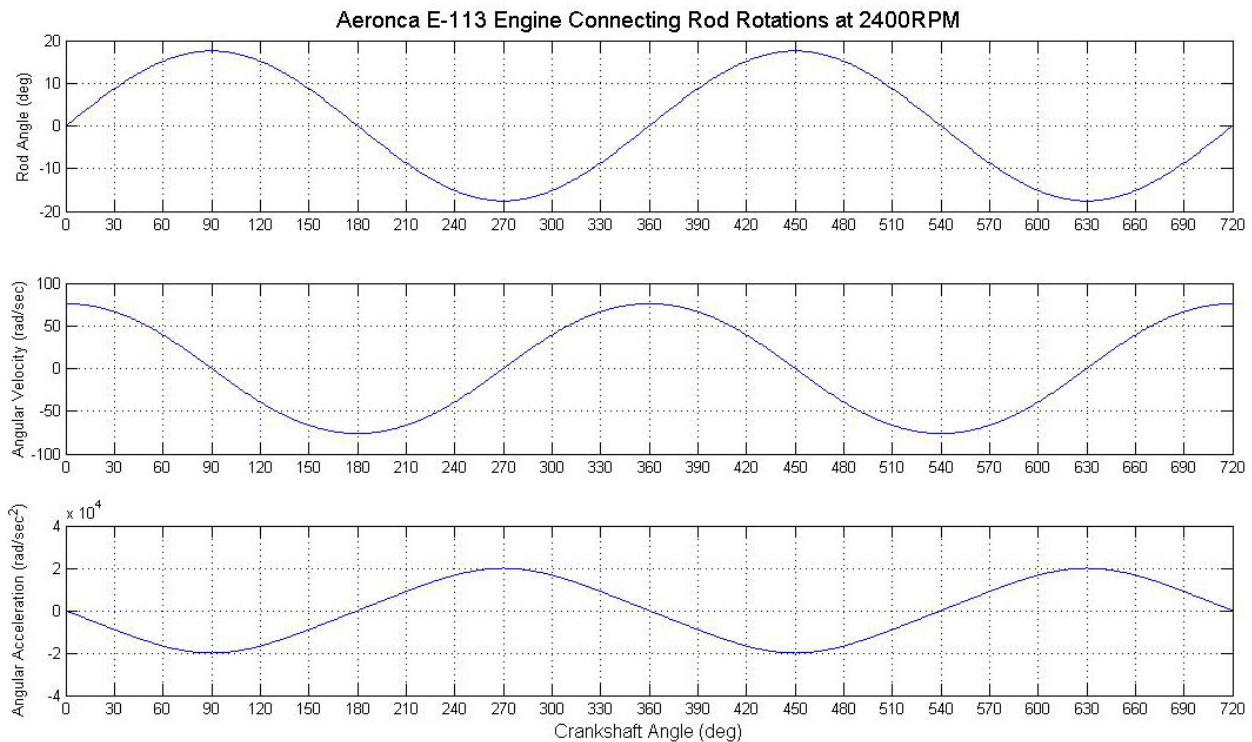


**Figure 4-4 Connecting rod kinematics including position, velocity, and acceleration**

## 4.3 Piston Forces

Figure 4-5 below shows the forces and accelerations applied to the piston. Considering the piston as a free body, an equation can be formulated by summing forces in the x and y directions. There are no moments to consider.

$$\sum Forces_x = F_p - F_G = M_p \cdot A_x$$

$$\sum Forces_y = F_w - F_s = 0$$

Solving for  $F_p$  and  $F_s$ ,

$$F_p = F_G + M_p \cdot A_x \quad \text{eq. (4-7)}$$

$$F_s = F_w \quad \text{eq. (4-8)}$$

Where

- $F_p$  = Horizontal force exerted by the piston (including inertial)
- $F_G$  = Force exerted by the gas pressure over the piston area
- $F_w$  = Vertical reaction of cylinder wall
- $F_s$  = Vertical connecting rod force
- $M_p$  = Mass of the piston
- $A_x$  = Acceleration along the cylinder axis

Under the conditions of constant engine speed of 2400RPM and no gas pressure the following plot in Figure 4-6 shows the inertial forces produced by the reciprocating piston of 0.0695 slugs mass.

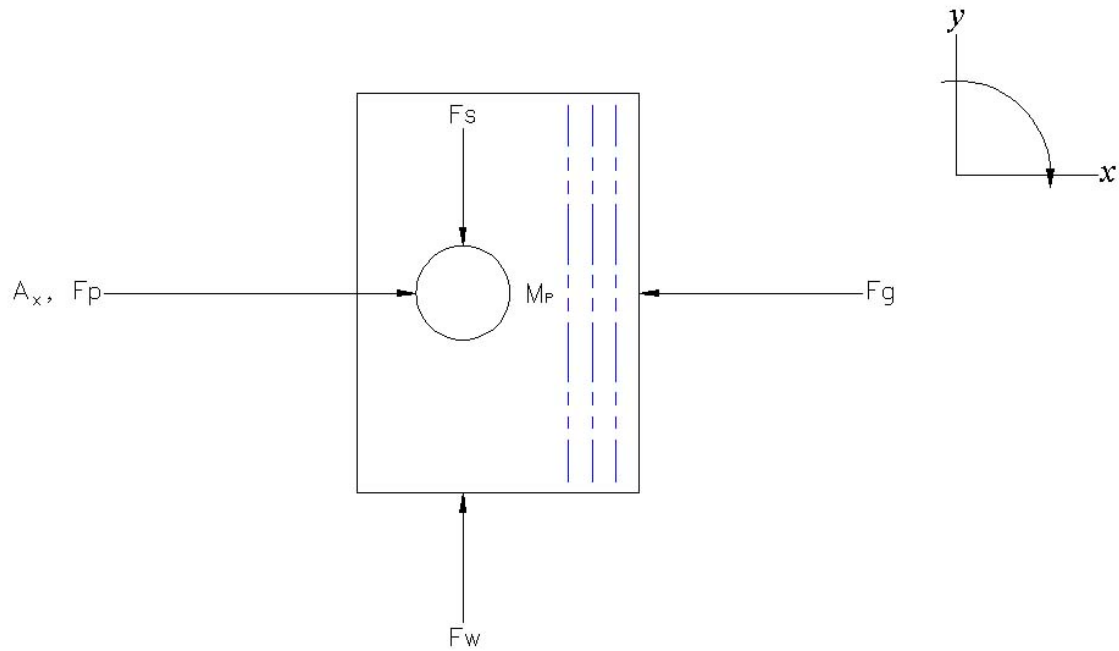


Figure 4-5 Free body diagram of piston showing applied forces and accelerations

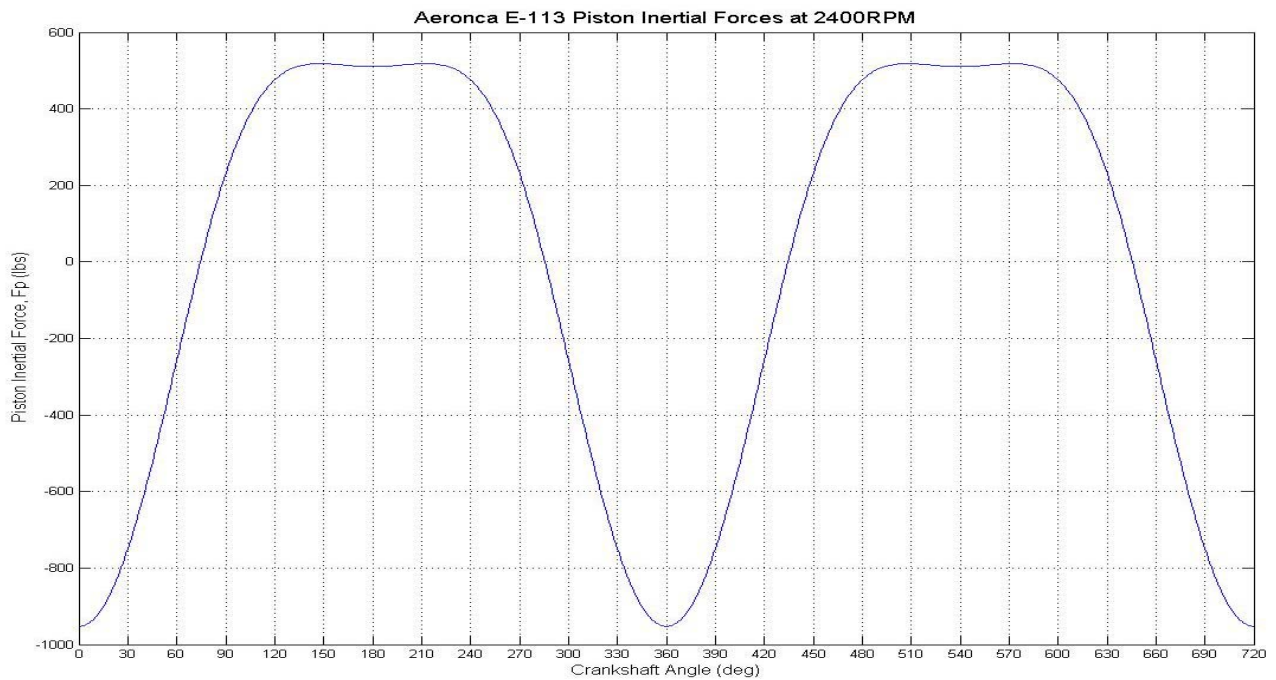


Figure 4-6 Inertial forces on a piston at 2400RPM

## 4.4 Connecting Rod Forces

The connecting rod serves to transmit the linear piston motion to a rotating crankshaft motion. As such, it exhibits both translational and rotational motion. Figure 4-7 below indicates the forces and accelerations imposed on the connecting rod. Again, taking the connecting rod as a free body and summing forces on the piston pin and crank pin, and moments about the piston pin, the following set of equations were developed.

$$\sum \text{Forces}_X = F_X - F_P = M_R (A_X + \omega_b^2 L_2 \cos \theta_b + \alpha_b L_2 \sin \theta_b)$$

$$\sum \text{Forces}_Y = F_Y + F_S = M_R (-\omega_b^2 L_2 \sin \theta_b + \alpha_b L_2 \cos \theta_b)$$

$$\sum \text{Moments}_O = F_X L \sin \theta_b + F_Y L \cos \theta_b = -M_R (A_X L_2 \sin \theta_b) + \alpha_b (I_R + M_R L_2^2)$$

Where

- $F_X$  = Horizontal force exerted by the crank pin
- $F_Y$  = Vertical force exerted by the crank pin
- $F_S$  = Vertical force exerted by the piston pin
- $I_{RO}$  = Moment of inertia about piston pin
- $I_R$  = Moment of inertia about center of mass
- $M_R$  = Mass of connecting rod
- $\omega_b$  = Angular velocity of connecting rod
- $\alpha_b$  = Angular acceleration of connecting rod

Solving for  $F_X$ ,  $F_Y$ , and  $F_S$ ,

$$F_X = F_P + M_R (A_X + \omega_b^2 L_2 \cos \theta_b + \alpha_b L_2 \sin \theta_b) \quad \text{eq. (4-9)}$$

$$F_Y = \frac{-M_R (A_X L_2 \sin \theta_b) + \alpha_b (I_R + M_R L_2^2)}{L \cos \theta_b} - \frac{F_X L \sin \theta_b}{L \cos \theta_b} \quad \text{eq. (4-10)}$$

$$F_S = -F_Y + M_R (-\omega_b^2 L_2 \sin \theta_b + \alpha_b L_2 \cos \theta_b) \quad \text{eq. (4-10A)}$$

Notice that eq. (4-10) is solved by substituting the previously determined  $F_X$  from eq. (4-9), and eq. (4-10A) is solved by substituting  $F_Y$  from eq. (4-10). MATLAB<sup>®</sup>

was used to provide the above manipulations and there was no need to display the lengthy results here.

Figure 4-8 below shows a plot of the forces in the  $F_x$ ,  $F_y$ , and  $F_s$  imposed upon the rod ends in turning the engine at a constant 2400RPM. Since the mass of the piston is 0.0695 slugs and the mass of the connecting rod is 0.0583 slugs, the horizontal inertial forces are almost doubled as compared to those in figure 4-6 for the piston only.

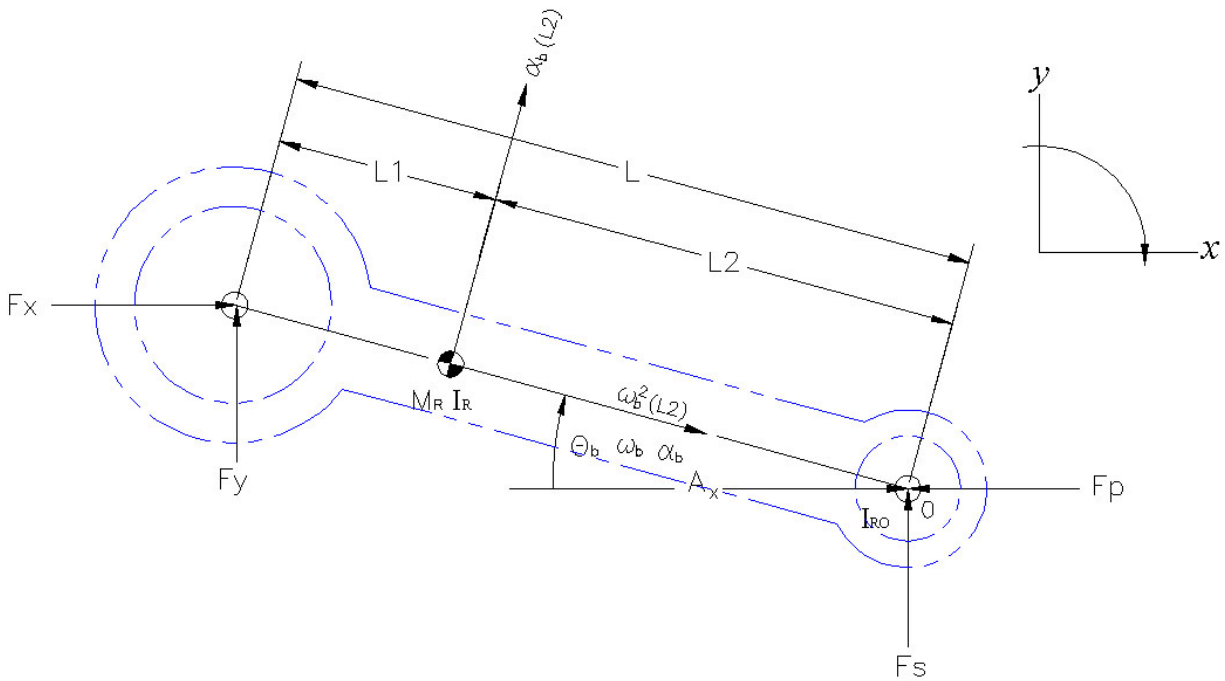


Figure 4-7 Free-body diagram of connecting rod forces and accelerations



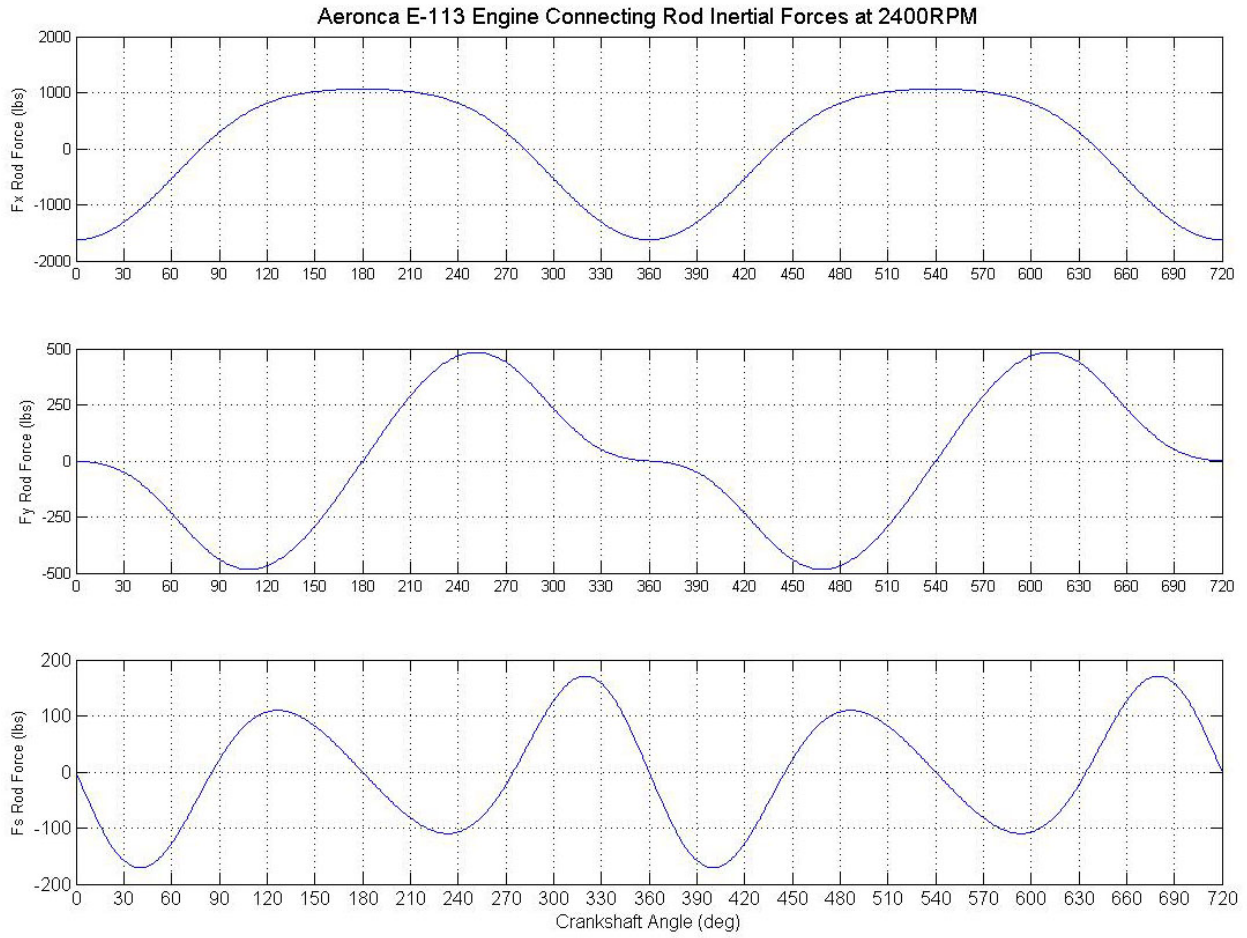


Figure 4-8 Connecting rod inertial forces at 2400RPM

## 4.5 Crankshaft Forces

Figure 4-9 below shows the forces imposed on the crankshaft by the connecting rod and the reaction at the main bearings. The rotational torque is taken out of the engine by the output shaft and applied to the propeller which consumes some power to drive the aircraft and stores some as kinetic energy to be returned to the engine to drive the compression stroke.

In analyzing the free-body diagram of the crankshaft, the following set of equations can be written.

$$\begin{aligned}\sum Forces_x &= F_H - F_X = M_{CW}(\omega_a^2 K_{CW} \cos \phi_a + \alpha_a K_{CW} \sin \phi_a) \\ \sum Forces_y &= F_V - F_Y = M_{CW}(\omega_a^2 K_{CW} \sin \phi_a - \alpha_a K_{CW} \cos \phi_a) \\ \sum Moments &= F_X R \sin \phi_a - F_Y R \cos \phi_a - T = (I_C + I_P + I_{CW})\alpha_a\end{aligned}$$

But  $I_{CW} = M_{CW} \cdot K_{CW}^2$  eq. (4-11)

Where  $F_H$  = Horizontal main bearing force  
 $F_V$  = Vertical main bearing force  
 $T$  = Engine output torque  
 $K_{CW}$  = Radius of gyration of counter weight (2.613 in)  
 $M_{CW}$  = Mass of counter weight (0.0665 slugs)  
 $I_{CW}$  = Moment of inertia of counter weight  
 $I_C$  = Moment of inertia of crankshaft  
 $I_P$  = Moment of inertia of propeller

Solving for  $F_H$ ,  $F_V$ , and  $T$ ,

$$F_H = F_X + M_{CW}(\omega_a^2 K_{CW} \cos \phi_a + \alpha_a K_{CW} \sin \phi_a) \quad \text{eq. (4-12)}$$

$$F_V = F_Y + M_{CW}(\omega_a^2 K_{CW} \sin \phi_a - \alpha_a K_{CW} \cos \phi_a) \quad \text{eq. (4-13)}$$

$$T = F_X R \sin \phi_a - F_Y R \cos \phi_a - (I_C + I_P + I_{CW})\alpha_a \quad \text{eq. (4-14)}$$

As can be seen in the last equation eq. (4-14) above, the rotational inertia of the counterweights have been separated from the crankshaft inertia even though they comprise one assembly. The counterweights are bolted onto the crankshaft and therefore removable. The assumption is made that all of the balancing function resides with the counterweights, even though the crankshaft probably aids or detracts from the net state of balance. For the current exercise the crankshaft is considered balance-neutral allowing the effect of altering counterweight mass to be observed. For most engines, the crankshaft and counterweights are one and the current distinction would not be possible.

Figure 4-10 below shows the horizontal (x-axis) component of connecting rod force applied to the crank pin, the horizontal component of counterweight force on the main bearing, and the combined effect of both acting together on the main bearings. As can be seen, the first two act in opposition and the bearing load is less than if the connecting rod force were totally reacted by the bearings.

In Figure 4-11 below, a hypothetical situation is investigated where the counterweight has a 1.5 times greater mass. As can be seen, the bearing loads are further reduced from above. It was found that adding more or less mass than the 1.5 times amount caused higher main bearing loads thereby indicating the optimum at that counterweight mass. The remaining unbalance is at two times the fundamental (second harmonic) which cannot be eliminated by crankshaft counterweights alone.

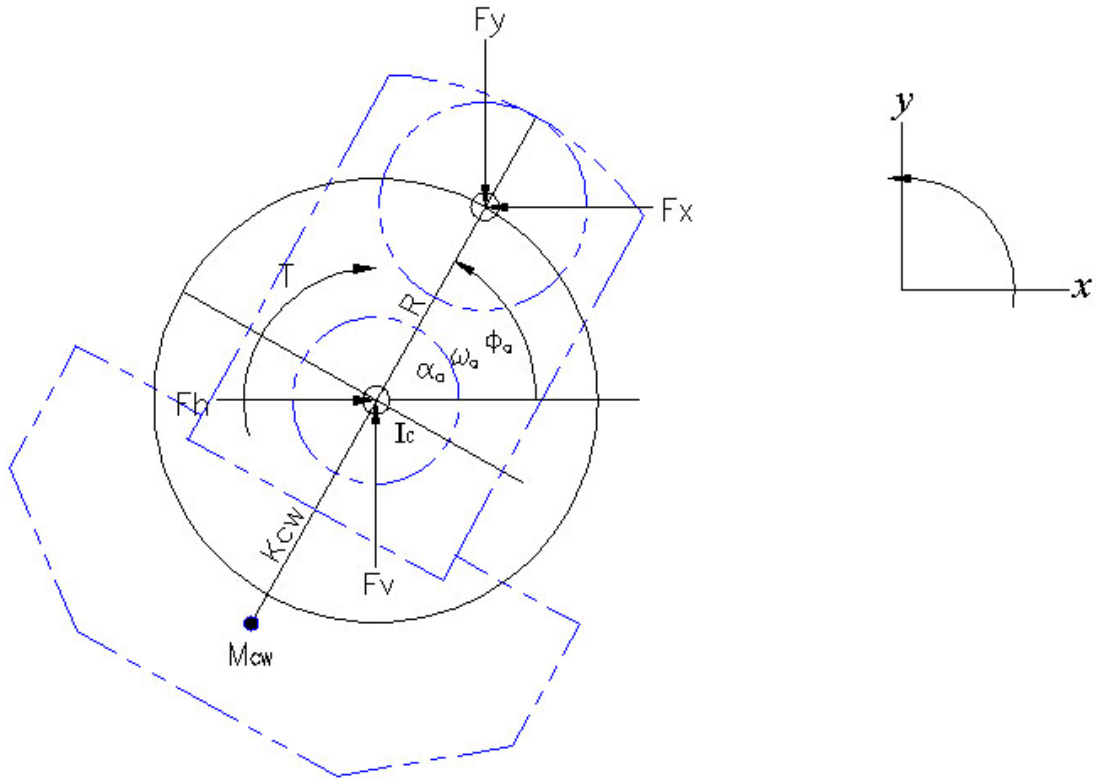


Figure 4-9 Free-body diagram of crankshaft forces and accelerations

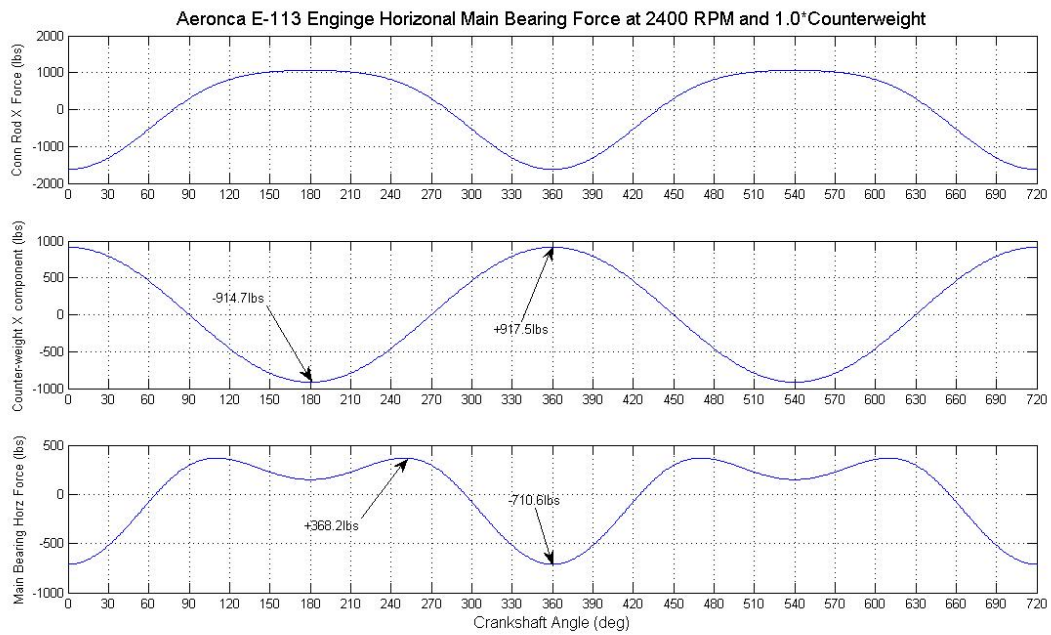


Figure 4-10 Horizontal crankpin and counterweight forces

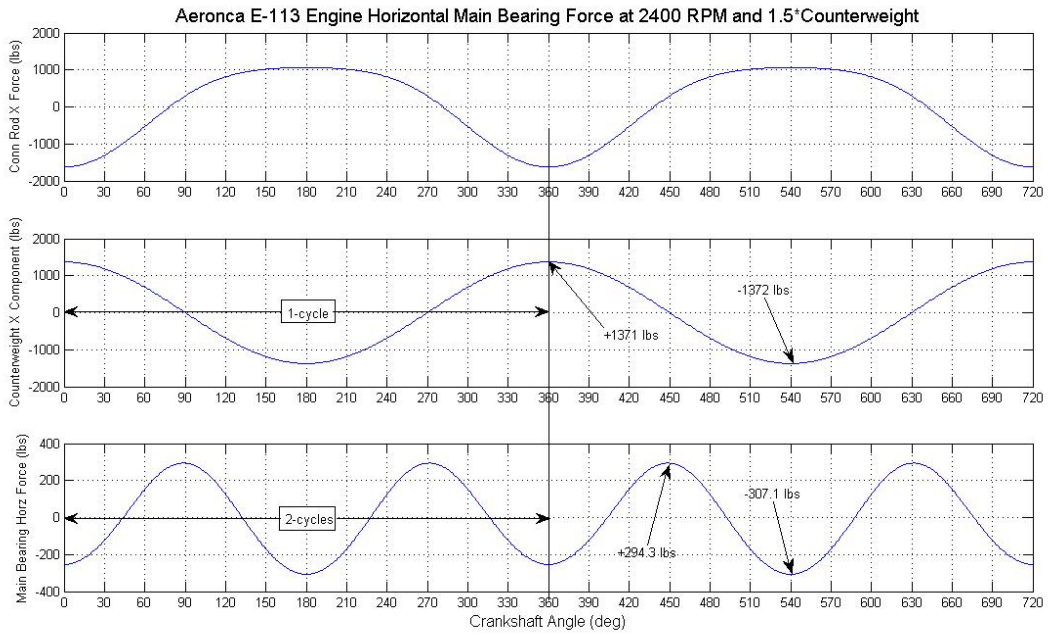


Figure 4-11 Horizontal crankpin and counterweight forces with 1.5 times the counterweight mass

## 4.6 Shaft Torque

The torque response is the result of a combination of gas pressures above the piston and inertial forces created by the rotating and reciprocating masses. Considering the crankshaft design task, the worst case scenario would involve the engine turning a heavy propeller. It is known that a wood propeller creates less stress on the crankshaft than a metal propeller due to differences in rotational mass. In stating a constant rotational speed of 2400RPM, the implication follows that the angular acceleration is zero ( $\alpha_a=0$ ) and a propeller of infinite moment of inertia is installed.

Repeating the equation above for torque and substituting eq. (4-9) for  $F_X$ , and eq. (4-10) for  $F_Y$ , and loading the piston pressure data shown in figure 3-4, the plot shown in figure 4-12 below is produced over two crankshaft revolutions,

$$T = F_X R \sin \phi_a - F_Y R \cos \phi_a - (I_C + I_P + I_{CW}) \alpha_a \quad \text{eq. (4-15)}$$

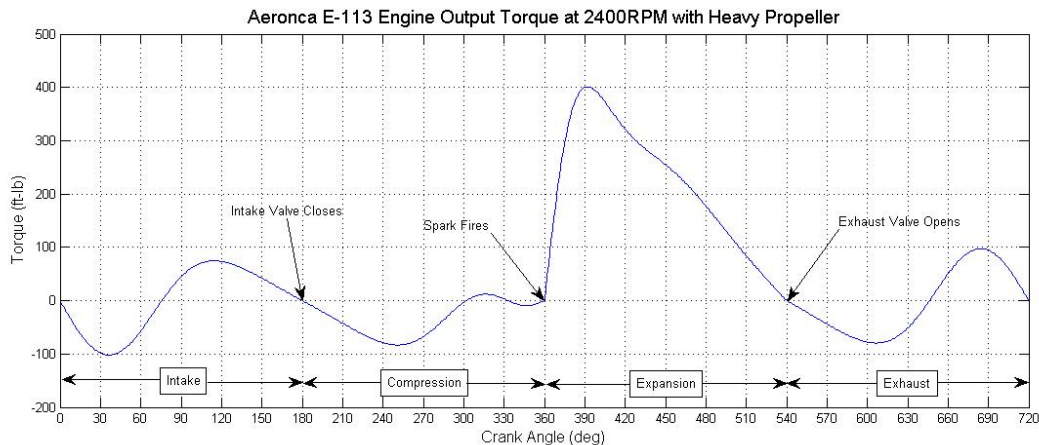


Figure 4-12 Crankshaft torque produced by a single cylinder

## 4.7 Two Cylinder Engine

The E-113 engine being considered is a twin cylinder, horizontally opposed, air-cooled, aircraft engine. Both cylinders operate identically except for being rotationally displaced out of phase. Since four engine strokes are completed in two revolutions (720°), even firing requires a phase difference between cylinders of 360°. The complete phase shift is accomplished by displacing the cylinders by 180° and displacing the crankshaft throws by 180°. As a result of this configuration, a high degree of inherent balance is achieved for the reciprocating masses since the pistons move in and out in opposition.

In considering the torque waveform produced above for one cylinder, the addition of the second cylinder would require that its waveform be delayed (or advanced) by 360° before its addition. Therefore the substitution of  $\Phi_a + 2\pi$  (or  $\Phi_a + 360^\circ$ ) is made for the second cylinder.

$$T_1 = F_x R \sin \phi_a - F_y R \cos \phi_a - (I_C + I_P + I_{CW}) \alpha_a$$

$$T_2 = F_x R \sin(\phi_a + 2\pi) - F_y R \cos(\phi_a + 2\pi) - (I_C + I_P + I_{CW}) \alpha_a$$

$$T_{TotEng} = T_1 + T_2$$

In making the above modification, the following plots in figure 4-13 were produced, with the bottom chart representing the combined torque response.

In averaging the instantaneous torque over 720° by numerical integration, the twin cylinder engine appears to produce 90.8 ft-lb of torque. However, the torque at the output shaft with losses taken into consideration should be:

$$T_{shaft} = (90.8 \text{ ft} - \text{lb}) \cdot (0.85) = 77.3 \text{ ft} - \text{lb} ,$$

indicating close agreement with the original premise taken from known engine specifications where:

$$T_{shaft} = \frac{P \cdot \frac{33,000 \text{ ft} - \text{lb} / \text{min}}{HP}}{2\pi \cdot N \text{ rev} / \text{min}} = \frac{36HP \cdot \frac{33,000 \text{ ft} - \text{lb} / \text{min}}{HP}}{2\pi \cdot 2400 \text{ rev} / \text{min}} = 78.8 \text{ ft} - \text{lb}$$

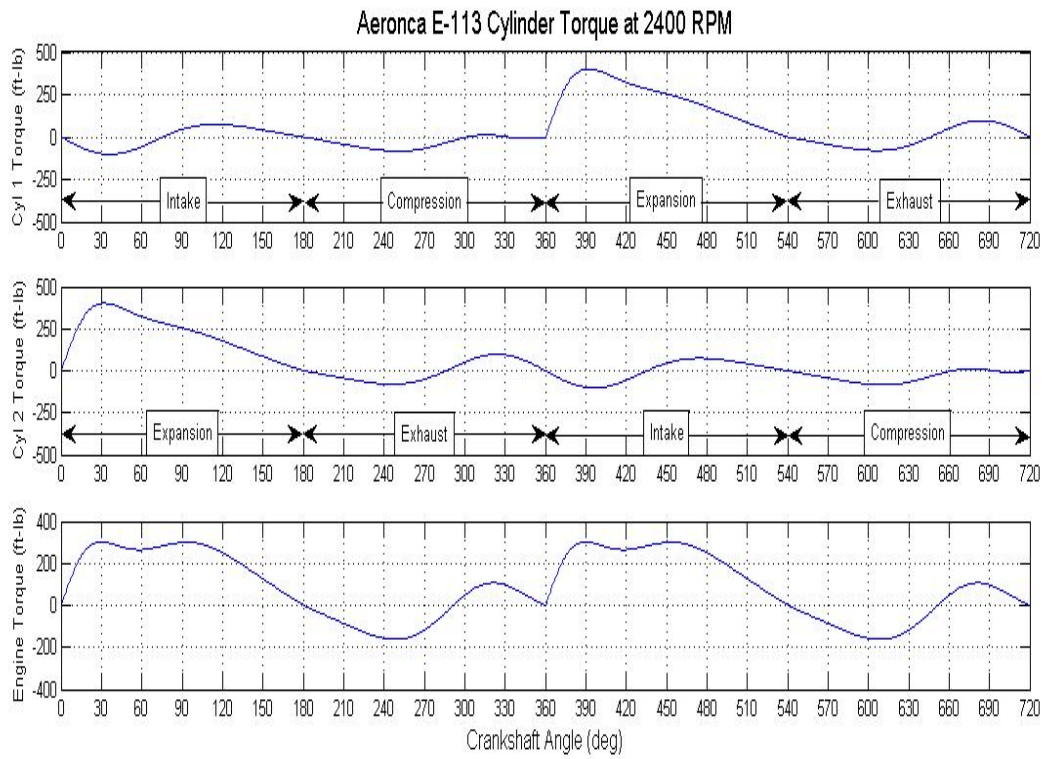


Figure 4-13 Crankshaft torque from twin cylinder engine at 2400RPM with rated piston pressures



## 4.8 Main Bearing Loads

In the case of output torque above, the two cylinder torque responses add algebraically. However, for the main bearing load, the forces subtract. With reference to the free body diagram in figure 4-14 below, the following relationships apply.

$$F_h = F_{X1} - F_{X2}$$

And  $F_v = F_{Y1} - F_{Y2}$

Where  $F_{X1} = F_p + M_R (A_X + \omega_b^2 L_2 \cos \theta_b + \alpha_b L_2 \sin \theta_b)$  eq. (4-16)

$$F_{Y1} = \frac{-M_R (A_X L_2 \sin \theta_b) + \alpha_b (I_R + M_R L_2^2)}{L \cos \theta_b} - \frac{F_X L \sin \theta_b}{L \cos \theta_b}$$
 eq. (4-17)

Forces  $F_{X2}$  and  $F_{Y2}$  have the same waveform as  $F_{X1}$  and  $F_{Y1}$  except displaced by  $360^\circ$ . Figure 4-15 below shows the phase shifted waveforms in the top two plots for the horizontal main bearing forces. The subtraction referred to above actually increases the bearing load due to the way the inertial and gas pressure forces from each cylinder combine.

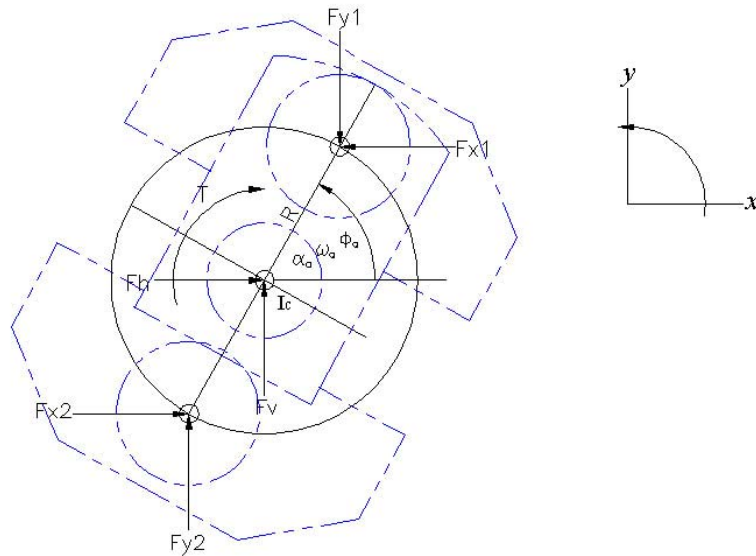


Figure 4-14 Free-body diagram of crankshaft reacting loads from both cylinders

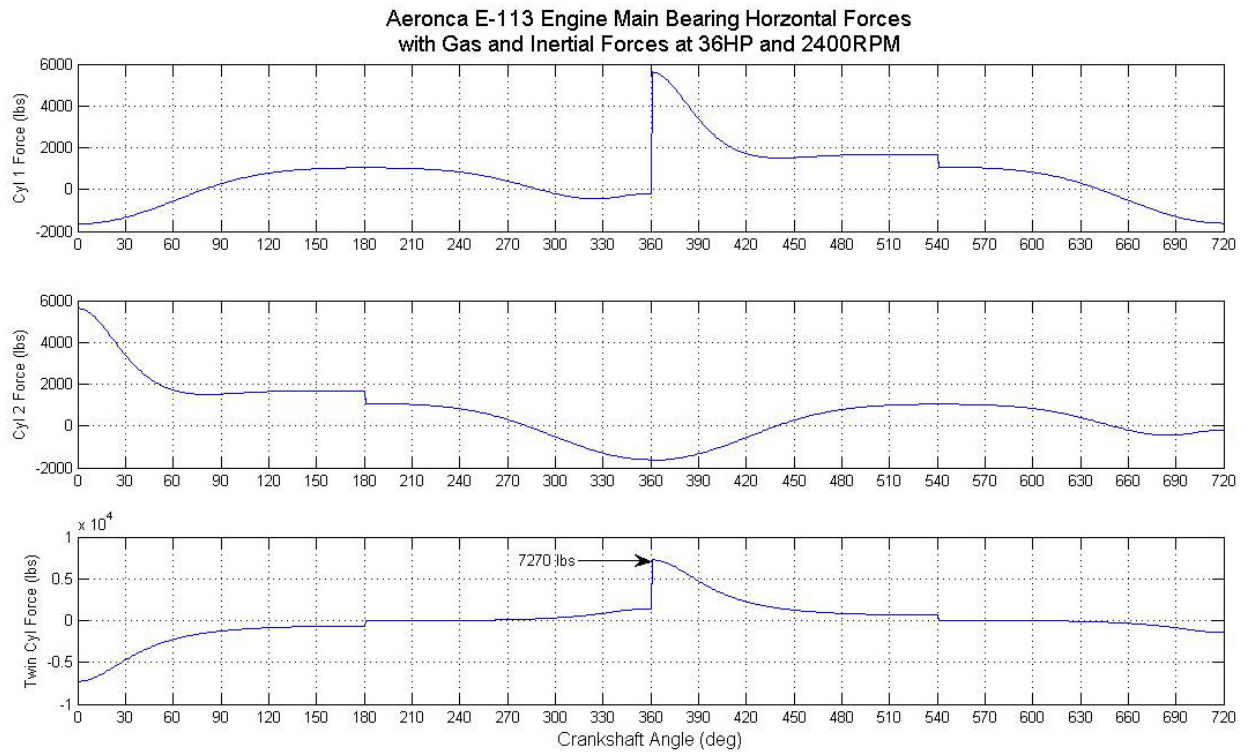


Figure 4-15 Horizontal main bearing forces for twin cylinder engine at rated power and 2400RPM

## 5.0 Conclusions

The objective of this thesis was to create a model for a propeller driven piston airplane engine that would be useful in designing the crankshaft and other dynamic components such as the piston and connecting rods. In providing an estimate of these loads, it must be remembered that the component strengths must be evaluated on the basis of fatigue strength. As such, the parameters of interest are magnitude of stress alternation and number of cycles. Methods are available to estimate the percent of damage produced by stress cycles over the endurance limit.

In order to make the analysis manageable, it was necessary to make several simplifying assumptions. These included the following:

1. The components are sufficiently rigid so that torsional resonance is not a factor. Of course, were oscillations present, the load cycles to failure would add quickly
2. The crankcase has infinite mass and does not move. Movement of the crankcase in response to internal forces would provide a cushioning effect. Therefore, this assumption provides higher forces than may actually be present.
3. The propeller provides sufficient flywheel effect that the angular velocity remains constant and the angular acceleration is nearly zero. Again, higher torsional loads are assumed than actually present resulting in an error to the conservative side.

Some limitations were found in the methods presented in this study. Since engine data was available for only the full throttle case (dynamometer curve Appendix A), generalizations to other power settings, such as 75% or 65% was not appropriate. Consideration was given to inserting lowering the intake manifold pressure values ( $p_a$ ), but the model would still not include losses in volumetric efficiency over the speed range.

Although considering the propeller as a heavy flywheel made a convenient simplification, developing the system of equations that allows a propeller of known moment of inertia would be preferable.

Some effects were not explicitly included such as engine friction, pumping losses, and gravity (or load factor). The friction effect was lumped into an engine efficiency coefficient when converting BMEP to IMEP. By modeling these effects separately, a higher fidelity simulation would be possible.

A large area of investigation left undone was that of crankshaft bending at the propeller hub. Gyroscopic forces due to abrupt maneuvers and uneven propeller disk loading due to sideslip will create bending load cycles at significant levels. Of course, aerobatic aircraft will feel this most greatly, but all other types will feel it to lesser degrees.

A more comprehensive study would have included the flight dynamics of the airplane. Appendix C discusses the flight parameters which affect engine loading. These include turning rates and accelerations, side slip and angle of attack, and thrust. Of course, including these effects would have greatly complicated this study. It is therefore left as promising material for a follow on investigation. An example of what can be done is given in Appendix D for the rather simple case of piston forces.

Lastly, you may know of the C-3 airplane and the E-113 engine as survivors of the Great Depression (1930's). As a minimal airplane, it was exactly what was needed at the time and became the model for generations of light aircraft. The original idea survives as the "Champ-Scout-Citabria-Decathlon" series. Apparently, the "goodness" of the original thought imbued an enduring effect. In researching the dynamics of the E-113, the feeling is one of finding the "holy grail" of inspirations. But the C-3/E-113 is said to have been inspired by the earlier Santos-Dumont "Demoiselle". In looking for the original idea, it appears like a thread running back in time, one idea building on another. Why choose the E-113 engine for the case study? For the same reason that we admire the "Citabria" airplane, an accessible aerobatic adaptation. Good ideas persist and continue to inspire us.

## List of References

## References

- [1] Angle, Glenn D., Engine Dynamics and Crankshaft Design, Aircraft Publications, New York, 1925.
- [2] “Piston Motion Equations”  
[http://en.wikipedia.org/wiki/Piston\\_motion\\_equations](http://en.wikipedia.org/wiki/Piston_motion_equations)
- [3] Heywood, John B., Internal Combustion Engine Fundamentals, McGraw-Hill Publishing Company, New York, 1988, pp. 42-49, 161-164, 173.
- [4] Taylor, Charles Fayette, The Internal-Combustion Engine in Theory and Practice Vol.2: Combustion, Fuels, Materials, Design, The M.I.T. Press, Cambridge, Mass, 1985.
- [5] Martin, George H., Kinematics and Dynamics of Machines, Waveland Press, Inc., Long Grove, IL, 1982.
- [6] Hardenbergh, Donald E., Introduction to Dynamics, Holt, Rinehart and Winston, Inc., New York, 1963.
- [7] Hibbeler, R.C. Engineering Mechanics – Dynamics, Macmillon Publishing Co., New York, 1989, pp. 319-320.
- [8] Higdon, Archie and William B. Stiles. Engineering Mechanics. Prentice-Hall, Inc., Englewood Cliffs, N.J., 1955. p. 251-252.
- [9] Aeronca Engine Handbook for the E-107A, E-113, E-113A, E-113B, E-113C Engines and Accessories, Aeronautical Corporation of America, Cincinnati, OH, 1938
- [10] Heldt, Peter Martin, High-Speed Combustion Engines, Chilton Company, 1956, pp.24-71.
- [11] Harker, R.J., “Fundamentals of Reciprocating Engine Dynamics”, University of Wisconsin, a paper.

- [12] Lichty, Lester C., Internal Combustion Engines, McGraw-Hill Book Co., New York, 1951, pp.480-521.
- [13] Lumley, John L., Engines: an Introduction, Cambridge University Press, 1999.
- [14] Montazersadgh, Farzin H. and Ali Fatemi, “Dynamic Load and Stress Analysis of a Crankshaft”, 2007, SAE International 2007-01-0258
- [15] Williams, Jonathan, and Ali Fatemi, “Fatigue Performance of Forged Steel and Ductile Cast Iron Crankshafts”, 2007, SAE International 2007-01-1001
- [16] Vinokurov, V. A., V. A. Kaminskii, V. A. Frost, and I. M. Kolesnikov, “Modeling of Combustion Processes in Internal Combustion Engines”, Chemistry and Technology of Fuels and Oils, Vol. 36, No. 6, 2000, UDC 662.62.629:665.65
- [17] Montazersadgh, Farzin H., and Ali Fatemi, “Optimization of a Forged Steel Crankshaft Subject to Dynamic Loading”, 2008 SAE International 2008-01-0432
- [18] Stoffels, Harald, “Dynamic effects of the power-conversion module in a reciprocating engine”, Arch Appl Mech DOI 10.1007/s00419-008-0261-2, 2008
- [19] Velts, V.L., and A.E. Kochura, “Dynamic Schematization of the Force Function of an Internal-Combustion Engine”, UDC 621.431.74:62-52/53
- [20] Nester, Tyler M., Alan G. Haddow, Steven W. Shaw, John E. Brevick, and Victor J. Borowski, “Vibration Reduction in a Variable Displacement Engine Using Pendulum Absorbers”, 2003, SAE International 2003-01-1484
- [21] Litak, Grzegorz, Tomasz Kamiński, Jacek Czarnigowski, Asok K. Sen, Mirosław Wendeker, “Combustion process in a spark ignition engine: analysis of cyclic peak pressure and peak pressure angle oscillations”, Meccanica DOI 10.1007/s11012-008-9148-0, 2008
- [22] Teichmann, Frederick K., Fundamentals of Aircraft Structural Analysis, Hayden Book Company, Inc., New York, 1968. pp. 40-42.

- [23] Peery, David J. and J.J. Azar Aircraft Structures. McGraw-Hill, Inc., New York, 1982. pp. 411-418.
- [24] Moore, Holly. MATLAB for Engineers, Pearson Prentice Hall, Upper Saddle River, N.J., 2007.
- [25] Raymer, Daniel P., Aircraft Design: A conceptual Approach, American Institute of Aeronautics and Astronautics, Inc., Washington, D.C., 1989, pp. 463-464.
- [26] Hiscocks, Richard D., Design of Light Aircraft, R.D. Hiscocks, Vancouver, BC, Canada, 1995, pp.2-3.
- [27] Dommasch, Daniel O., Sydney S Sherby, Thomas F. Connolly, Airplane Aerodynamics, Pitman Publishing Corporation, New York, 1967
- [28] Nelson, Wilbur C., Airplane Propeller Principles, John Wiley & Sons, Inc., New York, 1944, pp. 1-35.
- [29] Abbott, Ira H., and Albert E. Von Doenhoff, Theory of Wing Sections, Dover Publications, Inc. New York, 1959, pp. 2-9.
- [30] Rice, M.S., Handbook of Airfoil Sections for Light Aircraft, Aviation Publications, Milwaukee, WI, 1971, p. 13.
- [31] Nelson, Robert C., Flight Stability and Automatic Control, McGraw-Hill Book Company, New York, 1989, pp. 83-95.
- [32] Etkin, Bernard, and Lloyd Duff Reid, Dynamics of Flight – Stability and Control, John Wiley & Sons, Inc., New York, 1996, pp. 93-114.
- [33] “Design to Prevent Fatigue” white paper by the SolidWorks Corporation posted on web at  
<http://www.owl.net.rice.edu/~mech403/HelpFiles/FatigueWhitePaper.pdf>
- [34] “Crankshaft Design”, JCR Developments,  
<http://www.jcrdevelopments.com/content/engineering/crankshafts.html>



- [35] Reynolds, Jonathan C., “Crankshaft Design and Analysis Package” Swansea Institute of Higher Education, Internet Paper <http://www.jcrdevelopments.com>
- [36] Selby, Samuel M. (Editor), CRC Standard Mathematical Tables, The Chemical Rubber Co., Cleveland, OH, 1965.
- [37] Halliday, David, and Robert Resnick, Physics I & II, John Wiley & Sons, Inc., New York, 1966.
- [38] Protter, Murray, H., and Charles B. Morrey, Jr., College Calculus with Analytic Geometry, Addison-Wesley Publishing Company, Inc., Reading, Mass., 1964.
- [39] Wark, Kenneth, Thermodynamics, McGraw-Hill, Inc., New York, 1966, p. 113, 231.
- [40] McCallum, Miles, “The Technology Chasm”, Flyer, January 2005, pp. 28-35.
- [41] Kennedy, B., “What is BMEP???” , BEMP Fuel & Tuning , [http://www.bmepfuelandtuning.com/html/what\\_is\\_bmep\\_.html](http://www.bmepfuelandtuning.com/html/what_is_bmep_.html)

## Appendices

APPENDIX A

Dynamometer Data

Type..... 2 Cyl. Horizontal Opposed, overhead valves - air cooled.  
 Weight complete..... 115 lbs. including magneto, carburetor and hub.  
 Rated H. P..... 36 at 2400 R.P.M.  
 Cylinder Bore..... 4-1/4 inches.  
 Stroke..... 4 inches.  
 Total Displacement.. 113.5 cu. in.  
 Compression Ratio... 5.2 to 1  
 Direction of Rotation of Crankshaft - Counter clockwise (facing propeller).  
 Direction of Rotation of Magneto - Clockwise (facing propeller).  
 Direction of Rotation of Tachometer Shaft - Clockwise (facing rear of engine).  
 Magneto speed..... 1/2 crankshaft speed.  
 Camshaft speed..... 1/2 crankshaft speed.  
 Tachometer speed.... 1/2 crankshaft speed.  
 Oil pump..... 1/2 crankshaft speed.  
 Magneto..... Bosch, two spark.  
 Spark Plugs..... Aircraft Metric - 18 M.M. - Med. Cold.  
 Spark Plugs Gap.... .015 inches.  
 Oil Pressure..... 20 lbs. at 120°F.  
 Oil Temperature.... (Min.) 90°F before taking off. (Max.) 160°F. hot summer day.  
 Oil Reservoir..... 3 qts. in crankcase.  
 Oil Recommended.... 120 seconds at 210°F. summer, 100 seconds at 210°F. winter.  
 Oil consumption.... Cruising - 1/2 Pt. per hour.  
 Fuel consumption.... Cruising - 2-1/2 gals. per hour. Full throttle - 3 gals. per hour.  
 Fuel Recommended.... Aviation gasoline - 74 octane anti-knock rating or better - is approved with tetra-ethyl lead - 1 cc/gal. preferred. Should be straight run gasoline free from gum.  
 Carburetor..... Single, 1-1/2 Zenith.  
 Valve - Exhaust..... 1-25/32 diam. overall - 3/8 stem.  
 Valve - Inlet..... Same as exhaust valve.  
 Tappet clearance.... .005 on both valves with cold engine.  
 Valve adjustment... In rocker arm.  
 Valve Springs..... Two per valve. Same on both intake and exhaust.



Curves corrected to std. conditions -- 60°F carburetor air temperature - 29.92" Hg. barometer. Std. compression ratio -- aviation grade "85" gasoline.

Figure A-1 Manufacturer's performance Data

APPENDIX B

Engine Drawings

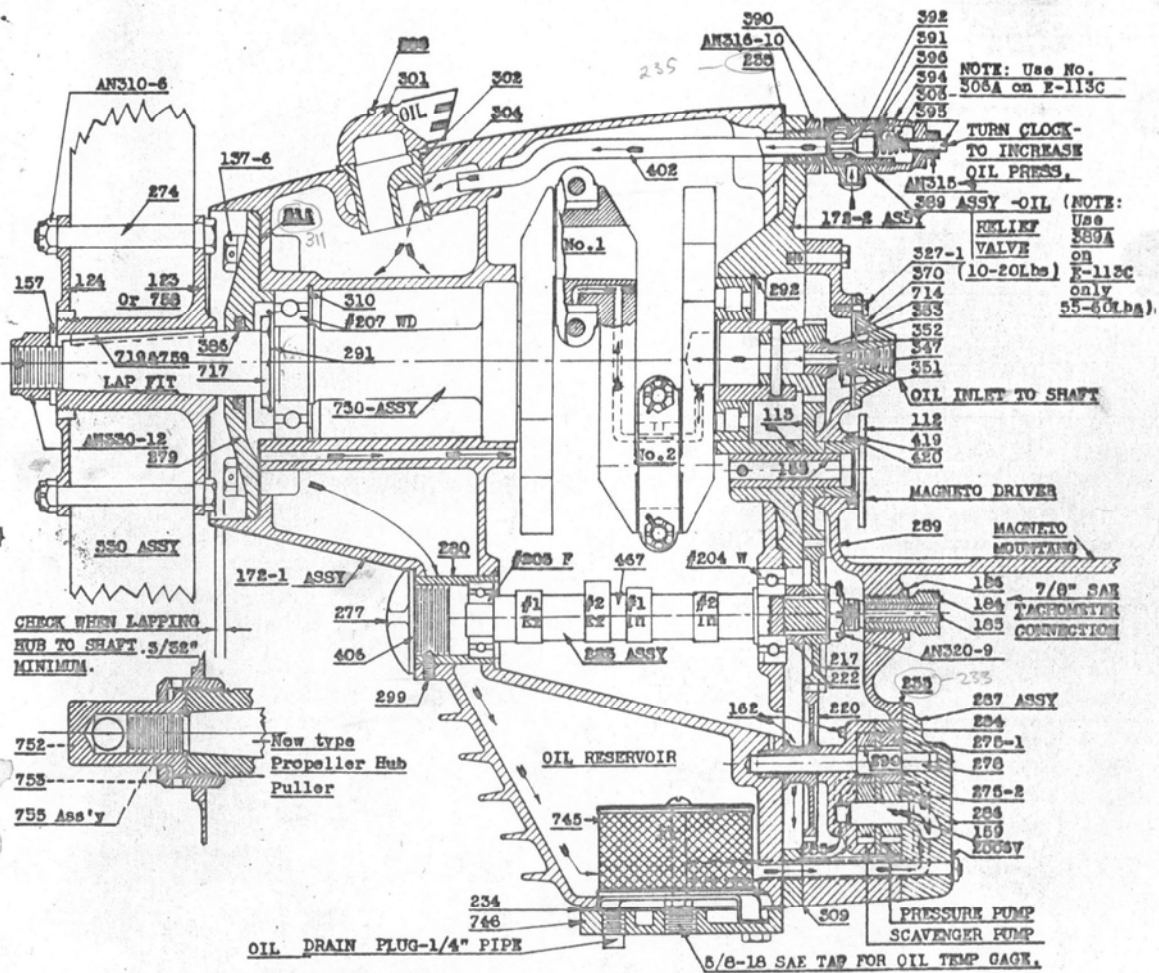


FIGURE 5 - BASIC ASSEMBLY AND OIL CIRCULATING SYSTEM - SIDE VIEW

Figure B-1 Engine assembly cross-section showing internal components

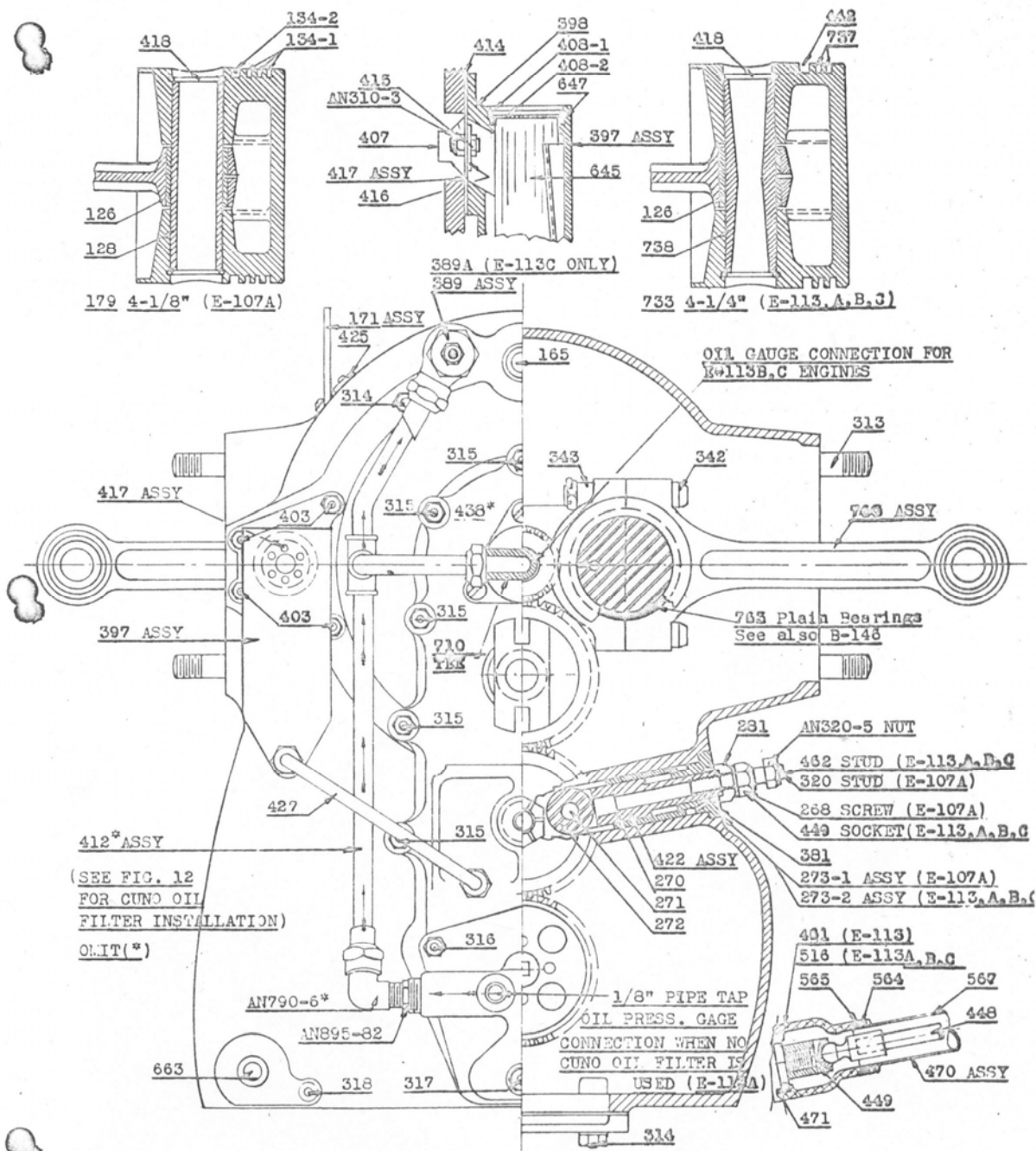


FIGURE 5 - BASIC ASSEMBLY AND OIL CIRCULATING SYSTEM - REAR VIEW

Figure B-2 Engine rear view showing back case parts and internal components

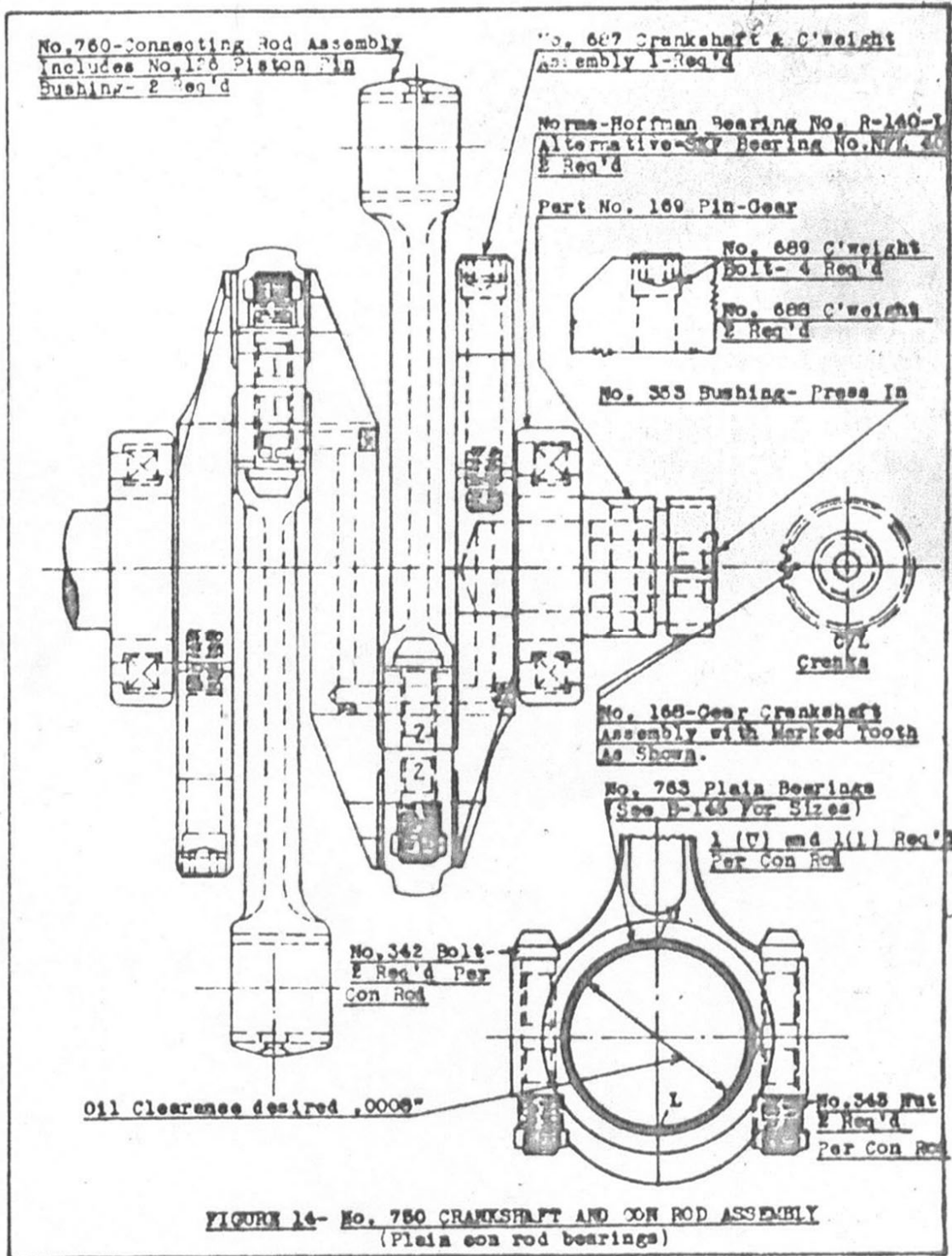


Figure B-3 Crankshaft and connecting rod assembly



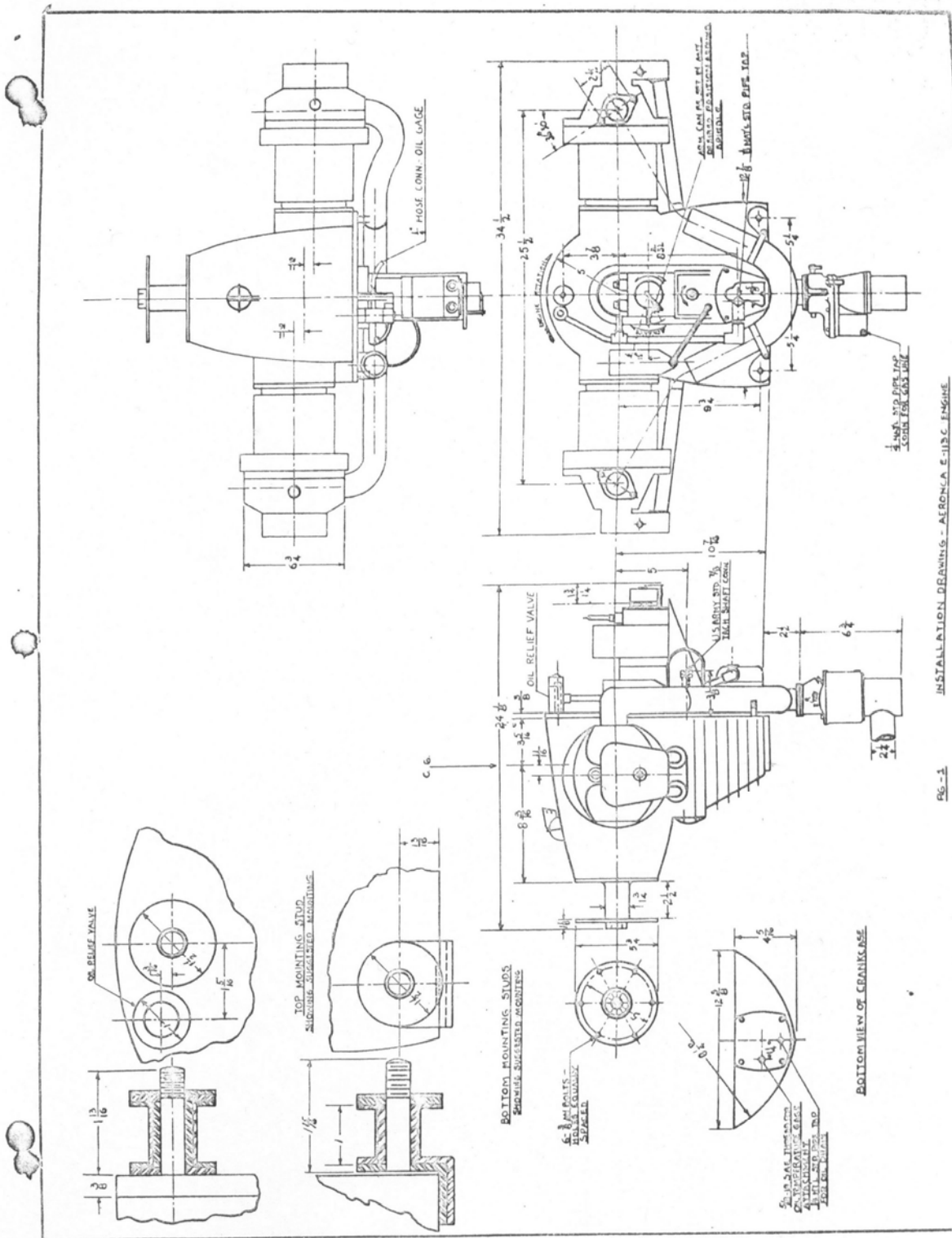


Figure B-4 Engine installation drawing showing overall dimensions

APPENDIX C

Flight Dynamics

## Flight Dynamics

An airplane in flight undergoes a variety of dynamic motions. In general, a system of twelve equations is required to fully describe the aerodynamic and inertial characteristics of the airplane, per Nelson [ ]. For the engine design task, however, we will assume the airplane exists, real or simulated, and the resulting range of linear and angular motions have been determined, say by flight testing. These values can be used in the equations developed to determine engine loads.

Figure C-1 below shows an airplane aligned within a Cartesian coordinate system indicating that subset of parameters that will have an influence on engine forces.

First considering translational effects, there are three linear accelerations along the three orthogonal axes ( $a_x$ ,  $a_y$ , and  $a_z$ ). Most significantly, the acceleration in the “z” direction is related to the load factor experienced by the airplane in turning flight, abrupt pull-ups, or push-over’s per Hiscocks [26]. When specified in units of gravity, the load factor is given by,

$$F_z = n \cdot W = Mng = Ma_z,$$

Similarly for accelerations parallel to the flight path due to sudden drag or power changes,

$$F_x = f \cdot W = Mfg = Ma_x$$

Where

$F_z$  = Force in the z-direction

$F_x$  = Force in the x-direction

$n$  = Vertical load factor  $L/W$

$f$  = Horizontal load factor  $D/W$  or  $T/W$

$g$  = Gravitational constant

$W$  = Weight of object or airplane

$M$  = Mass of object or airplane

The weight “W” can be that of the entire airplane as being sustained by the wings in flight, or it can represent an item of equipment contained inside the airplane, such as engine components. For coordinated flight the resulting force will always be directed in the positive “z” direction (down) with respect to the aircraft’s body axes.

About each axis the aircraft may be experiencing an angular turning rate during maneuvering flight. Rotations about the x, y, and z axis are termed roll, pitch, and yaw and are given symbols p, q, and r respectively. Being a rigid body, the angular motions will be present everywhere in the aircraft, however, they are considered to be positioned on the center of gravity (or center of mass) when the response of the airplane is being studied.

It is considered likely that the angular rates will have an effect on the pistons by changing their angular momentum as they move further from and closer to the center of the engine. The centrifugal forces created by the turning rates will produce additional loads on the engine components.

Gyroscopic forces will be likely on the propeller shaft and possibly the crankshaft bearings. With regard to the propeller, it is expected that a bending moment will be exerted on the extension shaft as it turns, and the crankshaft will impose additional forces on the main bearings due to gyroscopic forces.

In order to produce an angular rate, there must first be an angular acceleration. Assuming rotation about the aircraft's center of gravity, the effect will depend on the distance the engine is located from the center of gravity.

In cruising flight, the relative wind will be coming head-on to the propeller. During sideslip or pronounced angle of attack, the wind will encounter the propeller at an angle. The result will be that the blades will experience a higher angle of attack on half the disk, and a lower angle of attack of the other half. The result is the same for either sideslip or angle of attack and produces a bending moment on the extension shaft.

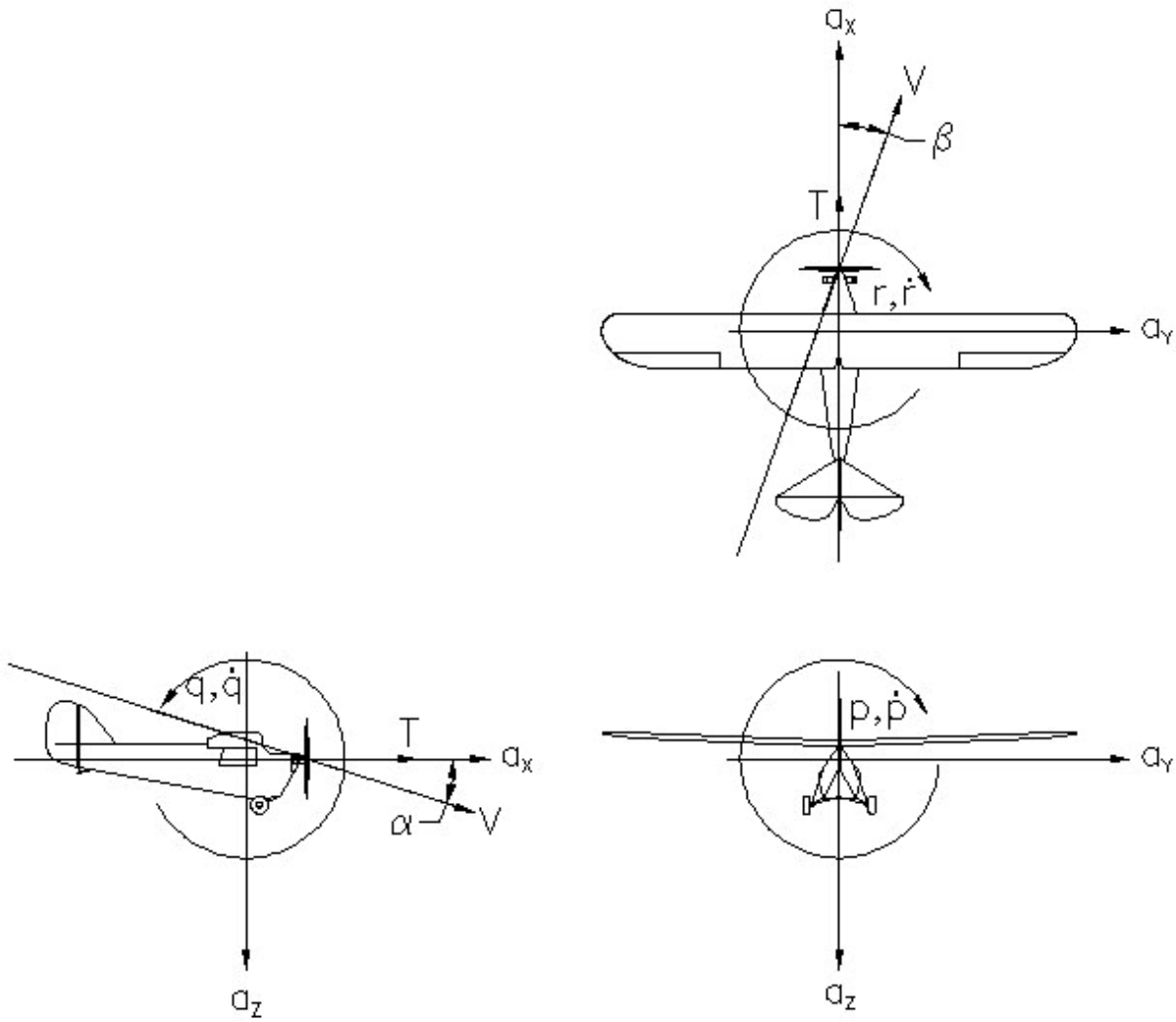


Figure C-1 Dynamic flight parameters which produce engine accelerations

## APPENDIX D

### Piston Forces in Dynamic Flight

## Piston Forces in Dynamic Flight

Figures D-1, D-2, and D-3 below show the forces and accelerations applied to the piston. Considering the piston as a free body, a set of equations can be formulated by summing forces in the x, y, and z directions and moments about a point. Notice that the current orientation of axes coincide with the body axes of the airplane as practiced by the field of stability and control. See figure C-1.

For left piston:

$$\sum Forces_Y = -F_R \cdot \cos \Omega_b + F_G = M_p(a_Y) - M_p(A_Y) + M_p(p^2 Y)$$

$$\sum Forces_Z = -F_{WZ} - F_R \cdot \sin \theta_b = M_p(a_Z) - M_p(\dot{p}Y) - M_p(2pV_Y)$$

$$\sum Moments = 0$$

For right piston:

$$\sum Forces_Y = F_R \cdot \cos \Omega_b - F_G = M_p(a_Y) + M_p(A_Y) - M_p(p^2 Y)$$

$$\sum Forces_Z = -F_{WZ} + F_R \cdot \sin \theta_b = M_p(a_Z) + M_p(\dot{p}Y) + M_p(2pV_Y)$$

$$\sum Moments = 0$$

Where

$F_G$  = Force exerted by the gas pressure over the piston area

$F_R$  = Connecting rod force directed along its line of action

$F_W$  = Vertical reaction of the cylinder wall on the piston

$M_p$  = Mass of the piston

$A_Y$  = Piston acceleration along the cylinder axis

$\theta_b$  = Connecting rod angle with respect to the cylinder axis

$V_Y$  = Piston velocity along the cylinder axis

$a_Z$  = Aircraft vertical acceleration

$p$  = Aircraft roll rate

$\dot{p}$  = Aircraft roll acceleration

For left piston:

$$\sum Forces_Y = -F_R \cdot \cos \Omega_b + F_G = M_P [(a_Y) - (A_Y) + (p^2 Y) + (\dot{r} d_L)]$$

$$\sum Forces_X = F_{WX} = M_P [a_X + \dot{r} Y + 2rV_Y - r^2 d_L]$$

$$\sum Moments = 0$$

For right piston:

$$\sum Forces_Y = F_R \cdot \cos \Omega_b - F_G = M_P [a_Y + A_Y - r^2 Y + \dot{r} d_R]$$

$$\sum Forces_X = F_{WX} = M_P [(a_X - \dot{r} Y - 2rV_Y - r^2 d_R)]$$

$$\sum Moments = 0$$

For left piston

$$\sum Forces_X = F_{WX} = M_P (a_X - q^2 d_L)$$

$$\sum Forces_Z = -F_{WZ} = M_P (a_Z - \dot{q} d_L)$$

For right piston

$$\sum Forces_X = F_{WX} = M_P (a_X - q^2 d_R)$$

$$\sum Forces_Z = -F_{WZ} = M_P (a_Z - \dot{q} d_R)$$

For the left piston the components of force in the x, y, and z directions can be combined for the following set of equations.

$$\sum Forces_X = F_{WX} = M_P (a_X + \dot{r} Y + 2rV_Y - r^2 d_L - q^2 d_L)$$

$$\sum Forces_Y = -F_R \cos \Omega_b + F_G = M_P (a_Y - A_Y + p^2 Y + r^2 Y + \dot{r} d_L)$$

$$\sum Forces_Z = -F_R \sin \Omega_b - F_{WZ} = M_P (a_Z - 2pV_Y - \dot{p} Y - \dot{q} d_L)$$



For the right piston,

$$\begin{aligned} \sum Forces_x &= F_{WX} = M_P (a_X - \dot{r}Y - 2rV_Y - r^2 d_R - q^2 d_R) \\ \sum Forces_y &= F_R \cos \Omega_b - F_G = M_P (a_Y + A_Y - p^2 Y - r^2 Y + \dot{r} d_R) \\ \sum Forces_z &= F_R \sin \Omega_b - F_{WZ} = M_P (a_Z + 2pV_Y + \dot{p}Y - \dot{q} d_R) \end{aligned}$$

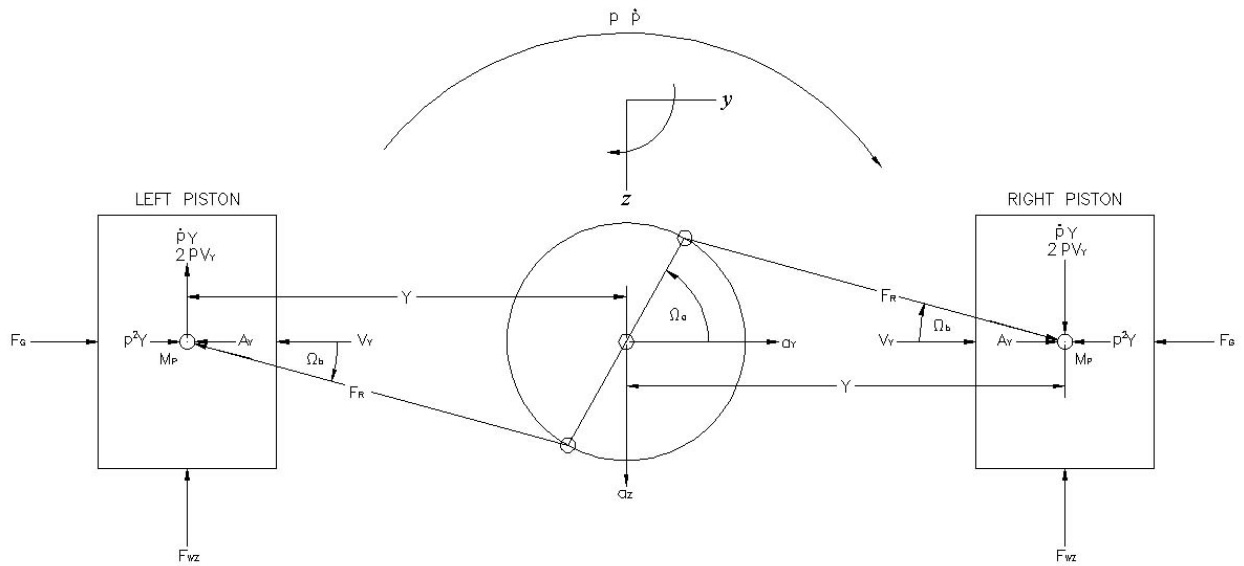


Figure D-1 Piston inertial forces during rolling flight

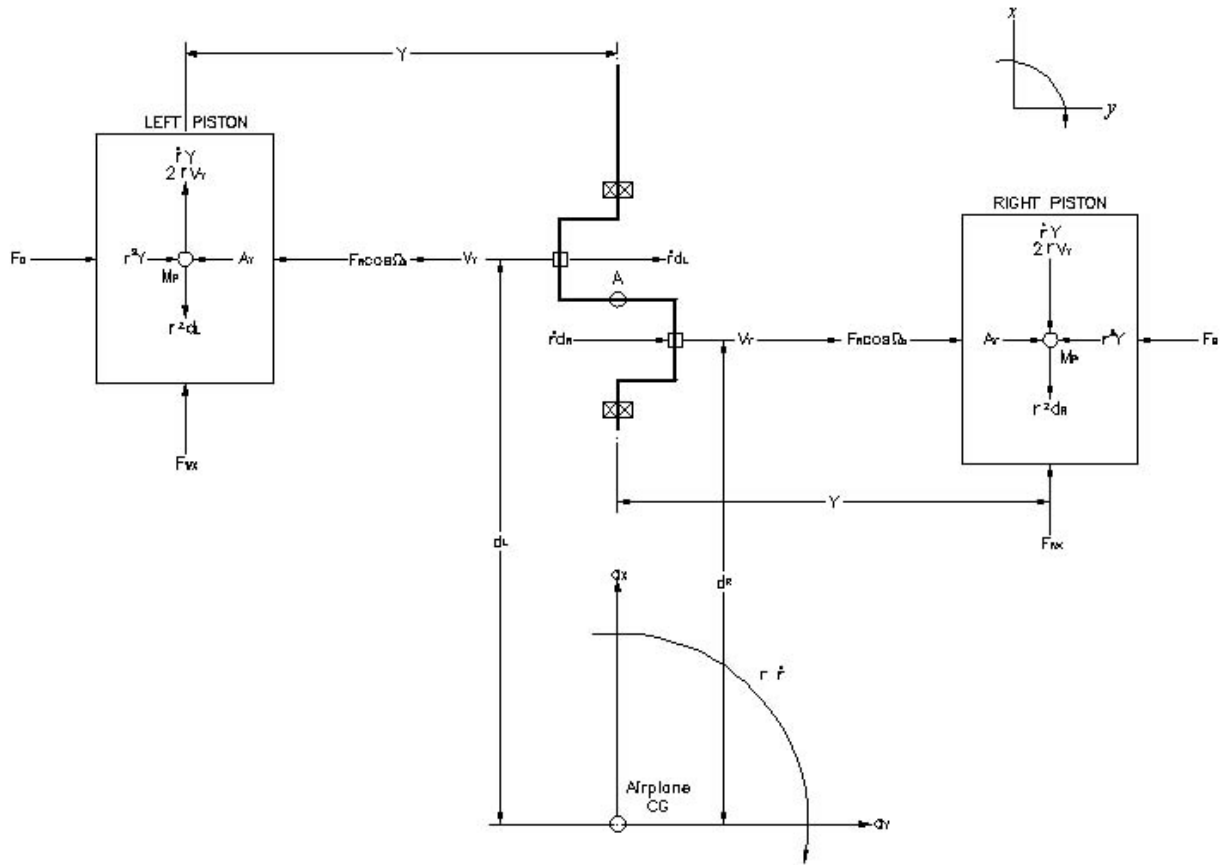


Figure D-2 Piston inertial forces during yawing flight

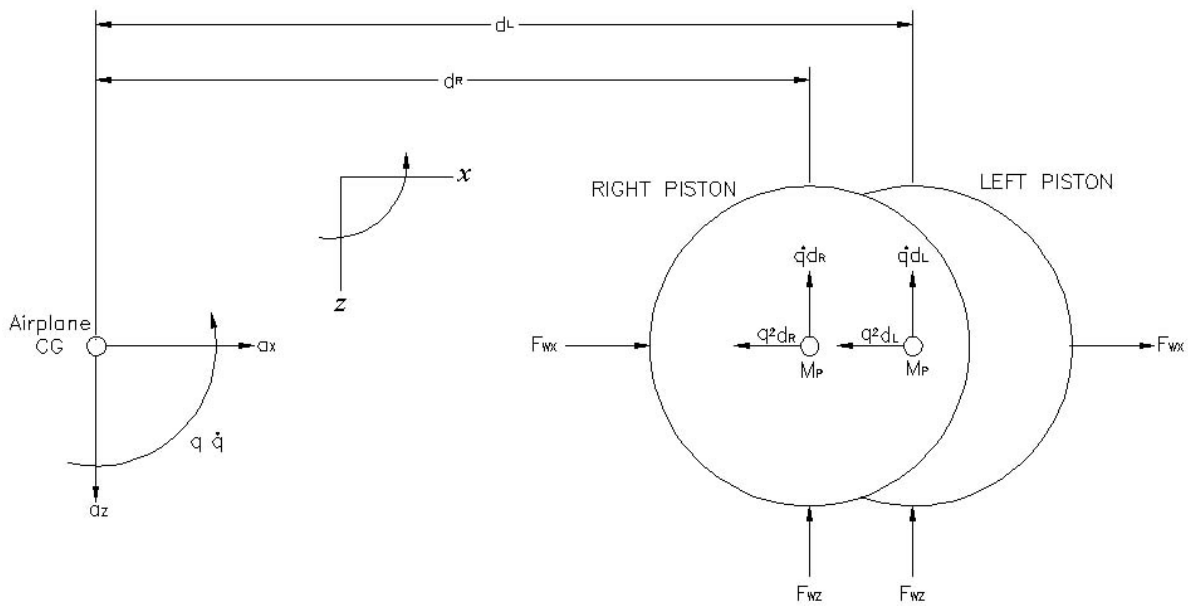


Figure D-3 Piston inertial forces during pitching flight

APPENDIX E  
MATLAB<sup>®</sup> Scripts

Figure E-1 Zload\_Parameters.m

```
%Loads measured and calculated dimensions, weights, and inertias and
%various repeatedly used parameters

d = (1:720);           %Crank angle in degrees
a = d*pi/180;         %Crank angle in radians
Wa = 2400*2*pi/60;    %Crank angular rate, rad./sec. (2400 RPM).
Aa = 0;               %Crank angular acceleration, rad./sec^2.
R = 2/12;             %Crank Pin radius, feet.
L = 6.625/12;         %Connecting rod length, feet.
L1 = 2.1717/12;       %Connecting rod CG from big end, ft.
L2 = (6.625-2.1717)/12; %Connecting rod CG from small end, ft.
Xcrank = R*cos(a);    %Crank arm horizontal projection, feet.
Ycrank = R*sin(a);    %Crank arm vertical projection, feet.
Xrod = (L^2-(R*sin(a)).^2).^0.5; %Connecting rod horizontal projection,
feet.
g = 32.174;           %Gravitational constant, ft./sec^2
Mrod = 1.875/g;        %Connection rod mass, lb-sec^2/ft.
Irod = 0.00318;       %Connecting rod I at CG, ft-lb-sec^2
Io_rod = Irod+L2^2*Mrod; %Connecting rod I at wrist pin
Mpiston = 0.0695;     %slugs
Rcw = 2.613/12;       %counterweight radius of gyration
Kcw = 2.613/12;       %counterweight radius of gyration
Mcw = 0.0665;%assume weight of 1 lb.
Icrank = 0.00695;
Iprop = 0.329;
PistonArea = (4.25/2)^2*pi;
Pa = 13;              %Intake pressure, psia
Pe = 15.7;            %exhaust pressure, psia
Cr = 5.4;              %compression ratio
Gamma = 1.3;
```

Figure E-2 Zpiston\_Kinematics.m

```
%This program determines the piston position X, Velocity Vx, and
%acceleration Ax
%
%
%
%
Zload_parameters

%%Piston Kinematics%%
X = 12*(Xcrank + Xrod);           %Crank center to wrist pin length, inch.
dx_da = -Ycrank -(0.5*R^2*sin(2*a))/Xrod; %Piston displacement vs Crank
angle displacement.
Vx = (dx_da)*Wa;                %Piston linear velocity, ft/sec.
d2x_da2 = -Xcrank - (R^2*cos(2*a))./Xrod - ((R^4/4)*(sin(2*a)).^2)./Xrod.^3;
%Piston displ. vs Crank< displ.
Ax = (d2x_da2)*Wa^2 + (dx_da)*Aa; %pin acceleration as function of time

figure (1)
subplot(3,1,1), plot (d,X), title('piston position, inch')
subplot(3,1,2), plot ( d,Vx)
title ('piston velocity, ft/sec')
subplot(3,1,3), plot (d,Ax)
title ('piston acceleration, ft/sec^2')
```

Figure E-3 Zrod\_kinematics.m

```
%Determines the connecting rod angle based of the crank angle,  
%the rod angular velocity Wb, and the angular acceleration Ab  
%  
%  
%  
%  
  
Zload_parameters  
  
%%%Rod Kinematics%%%  
b = asin(Ycrank/L);  
Wb = (Xcrank./Xrod).*Wa;  
Ab = (Xcrank.*Aa-Ycrank.*Wa.^2)./Xrod + (Xcrank.^2.*Ycrank.*Wa.^2)./Xrod.^3;  
  
figure (1)  
subplot(3,1,1), plot (d,b*180/pi);  
title('Rod Angle, (deg)')  
subplot(3,1,2), plot ( d,Wb)  
title('rod angular velocity, rad/sec')  
subplot(3,1,3), plot (d,Ab)  
title('rod angular acceleration, rad/sec^2')
```

## Figure E-4 Zindicator.m

```
%Produces the piston pressure "Pindicator" and piston force "Fgas"
%matrices

Zload_parameters

Pd = 58.7;
Vol = 25.793 + (8.625-X)*PistonArea*2;           %inch^3 total engine
                                                    %volume, including
                                                    %combustion chambers

figure (1)
plot(d,Vol)
ylabel('Volume')

Pcomp=Pa*(139.283./Vol).^Gamma;
Pexpan=Pd.*(139.283./Vol).^Gamma;

figure(2)
plot(d,Pcomp,d,Pexpan)

figure(3)
plot(Vol,Pexpan,'k')
hold on
plot(Vol,Pcomp,'k')
grid on
ylabel('cylinder pressure, psi')
xlabel('cylinder volume, cu.in.')
title('Aeronca E-113 Engine Indicator Diagram, 36HP/2400RPM')
axis([0 150 0 600])

%%%Gas Pressure Forces%%%
OneArray = ones(1,720);
Pintake = (Pa-14.7)*OneArray;           %intake
Pcompression = Pcomp-14.7;           %compression
Pexpansion = Pexpan-14.7;           %expansion
Pexhaust = (Pe-14.7)*OneArray;       %exhaust
Pindicator =
[Pintake(1:180),Pcompression(181:360),Pexpansion(361:540),Pexhaust(541:720)];
figure (4)
plot(d,Pindicator);
Fgas = Pindicator*PistonArea;
title('Piston Force'), xlabel('crankshaft Angle'), ylabel('pressure lbs')
```

## Figure E-5 Zpiston\_inertia.m

```
%Computes the inertial forces on the piston (no gas pressure)
%
%
Zload_parameters
Zpiston_kinematics
Zrod_kinematics
Fgas=0;

Fp=(Fgas+Mpiston.*Ax);

figure (3)
plot (d,Fp), title('Piston Inertial Force (lbs)')
```



Figure E-6 Zrod\_inertia.m

```
%determines inertial forces on the connecting rod with
%engine turning

Zload_parameters
Zpiston_kinematics
Zrod_kinematics

Fgas=0;

Fp=(Fgas+Mpiston.*Ax);

%Rod Forces
Fx=Fp + (Wb.^2.*L2.*cos(b) + Ab.*L2.*sin(b) + Ax).*Mrod;
Fy=(Mrod.*(Ax.*L2.*sin(b))+Ab.*(Irod+Mrod.*L2.^2)-Fx.*L.*sin(b))./L.*cos(b);
Fs=-Fy + (-Wb.^2.*L2.*sin(b) + Ab.*L2.*cos(b)).*Mrod;

figure (1)
subplot(3,1,1), plot (d,Fx), title('X Rod Force (lbs)')
subplot(3,1,2), plot ( d,Fy), title ('Y Rod Force (lbs)')
subplot(3,1,3), plot ( d,Fs), title ('S Rod Force (lbs)')
```

## Figure E-7 Zrod\_forces.m

```
%Determines forces (Fx, Fy, Fs) acting on the connecting rod
%due to inertial and gas pressure

Zload_parameters
Zindicator;
Zpiston_kinematics
Zrod_kinematics

Fp=(Fgas+Mpiston.*Ax);

%Rod Forces
Fx=Fp + (Wb.^2.*L2.*cos(b) + Ab.*L2.*sin(b) + Ax).*Mrod;
Fy=(Mrod.*(Ax.*L2.*sin(b))+Ab.*(Irod+Mrod.*L2.^2)-Fx.*L.*sin(b))./L.*cos(b);
Fs=-Fy + (-Wb.^2.*L2.*sin(b) + Ab.*L2.*cos(b)).*Mrod;

figure (1)
subplot(3,1,1), plot (d,Fx), title('X Rod Force (lbs)')
subplot(3,1,2), plot ( d,Fy), title ('Y Rod Force (lbs)')
subplot(3,1,3), plot ( d,Fs), title ('S Rod Force (lbs)')
```

Figure E-8 Zcrank\_forces.m

```
%Determines the Horizontal and Vertical Main bearing load and
%Shaft Torque produced in a single cylinder with both inertial
%and gas pressures applied
%
%
%
Zload_parameters;           %Loads dimensions, weights, inertias, etc.

Zindicator;                 %computes the piston force profile

Zpiston_kinematics         %Computes Piston position X, Velocity Vx, and
                           %acceleration Ax
Zrod_kinematics            %Computes Rod angle, angular velocity, and
                           %angular acceleration
Zrod_forces                 %Computes the Fx, Fy, and Fs forces

Fwall=Fs;                  %Cylinder wall force

%Crank Forces
Icw=Mcw*Kcw^2;
Fh=Fx+Mcw.*(Wa.^2.*Kcw.*cos(a)+Aa.*Kcw.*sin(a));
Fv=Fy+Mcw.*(Wa.^2.*Kcw.*sin(a)-Aa.*Kcw.*cos(a));
T=Fx.*R.*sin(a)-Fy.*R.*cos(a)-(Icrank+Iprop+Icw).*Aa;
Hcw=Mcw.*(Wa.^2.*Kcw.*cos(a));           %horz counterweight reaction
Vcw=Mcw.*(Wa.^2.*Kcw.*sin(a));           %horz counterweight reaction
figure (1)
subplot(3,1,1), plot (d,Fh), title('Horz Main Bearing Force (lbs)')
subplot(3,1,2), plot (d,Fv), title('Vert Main Bearing Force (lbs)')
subplot(3,1,3), plot (d,T), title('Shaft Torque (ft-lbs)')
```

## Figure E-9 Ztwin\_torque.m

```
%Computes the torque contribution from both cylinders firing
%360 degs out of phase

Zload_parameters
Zpiston_kinematics
Zrod_kinematics
Zrod_forces
Zcrank_forces

T1=T;
T2=[T1(361:720),T1(1:360)];
Teng=T1 + T2;
figure(1), plot(d,Teng);
subplot(3,1,1), plot(d,T1); title('left cyl')
subplot(3,1,2), plot(d,T2); title('right cyl')
subplot(3,1,3), plot(d,Teng); title('twin torque')

AvgTeng=sum(Teng)/720;           %average torque over two revolutions
```

## Figure E-10 Zmain\_bearing\_forces.m

```
%Computes main bearing forces on twin cylinder engine with  
%inertial and gas pressures
```

```
Zload_parameters  
Zindicator  
Zpiston_kinematics  
Zrod_kinematics  
Zrod_forces  
Zcrank_forces
```

```
Fx1=Fh;  
Fx2 = [Fx1(361:720),Fx1(1:360)];
```

```
Fy1=Fv;  
Fy2 = [Fy1(361:720),Fy1(1:360)];
```

```
Fhh=Fx1-Fx2;  
Fvv=Fy1-Fy2;
```

```
figure(11)  
subplot(3,1,1), plot(d,Fx1); title('Left horz force')  
subplot(3,1,2),plot(d,Fx2); title('right horz force')  
subplot(3,1,3),plot(d,Fhh); title('combined horz force')
```

```
figure(12)  
subplot(3,1,1), plot(d,Fy1); title('Left vert force')  
subplot(3,1,2),plot(d,Fy2); title('Right vert force')  
subplot(3,1,3),plot(d,Fvv); title('combined vert force')
```

## APPENDIX F

### Pictures



Figure F-1: Aeronca E-113 airplane engine dynamic components including the pistons, connecting rods, and crankshaft shown with the propeller hub mounted

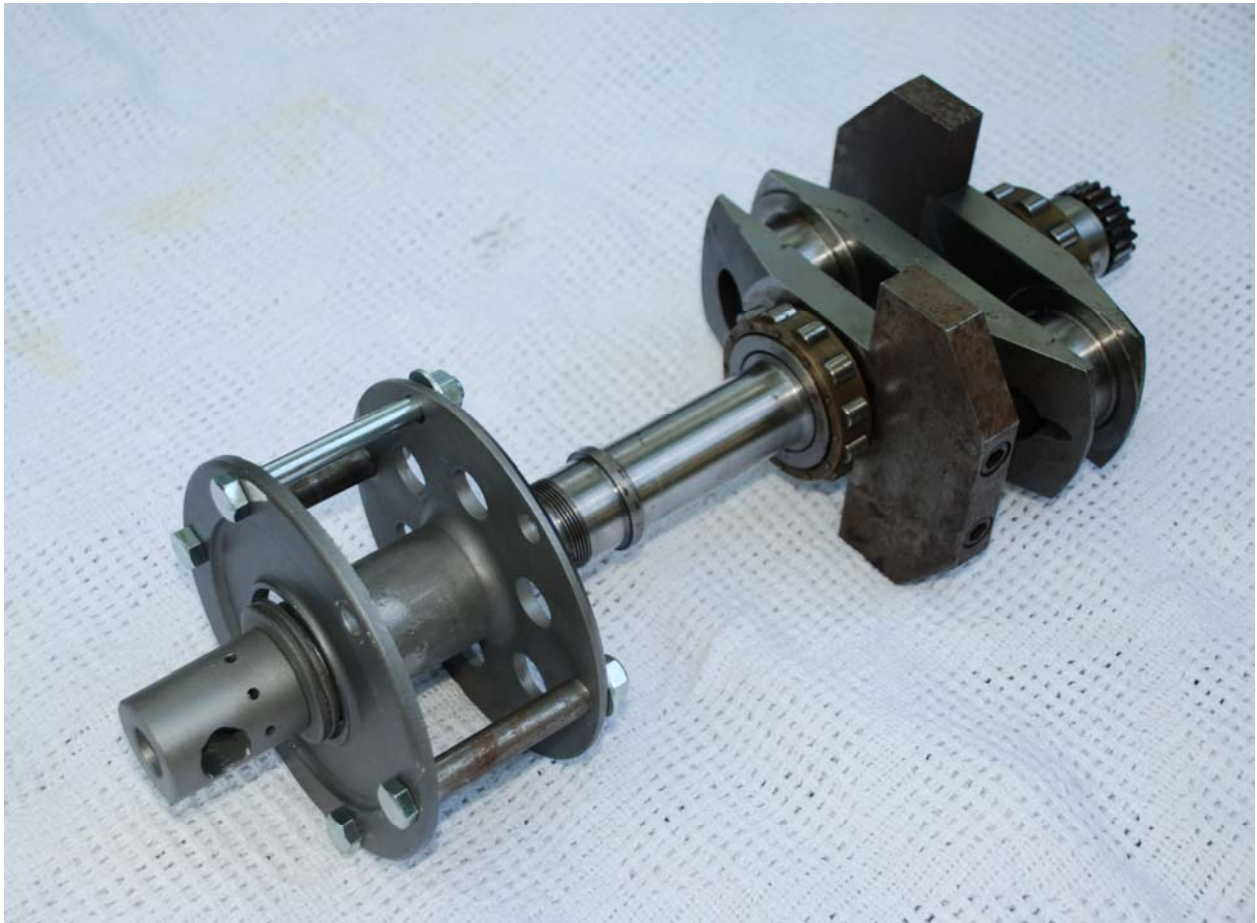


Figure F-2: Aeronca E-113 crankshaft assembly consisting of the forged crank, the main roller bearings, propeller hub and nut, and bolted-on counterweights



Figure F-3: Back view of crankshaft assembly showing oil spindle hole, timing gear, main bearing, and counterweights



Figure F-4: Fixture for swinging the crankshaft assembly to determine the moment of inertia by supporting on knife edge through the crank pin lightening hole





Figure F-5: Forged connecting rod pair with bronze wrist pin bushings, split Babbitt crank pin bearing, and close tolerance clamp bolts/nuts

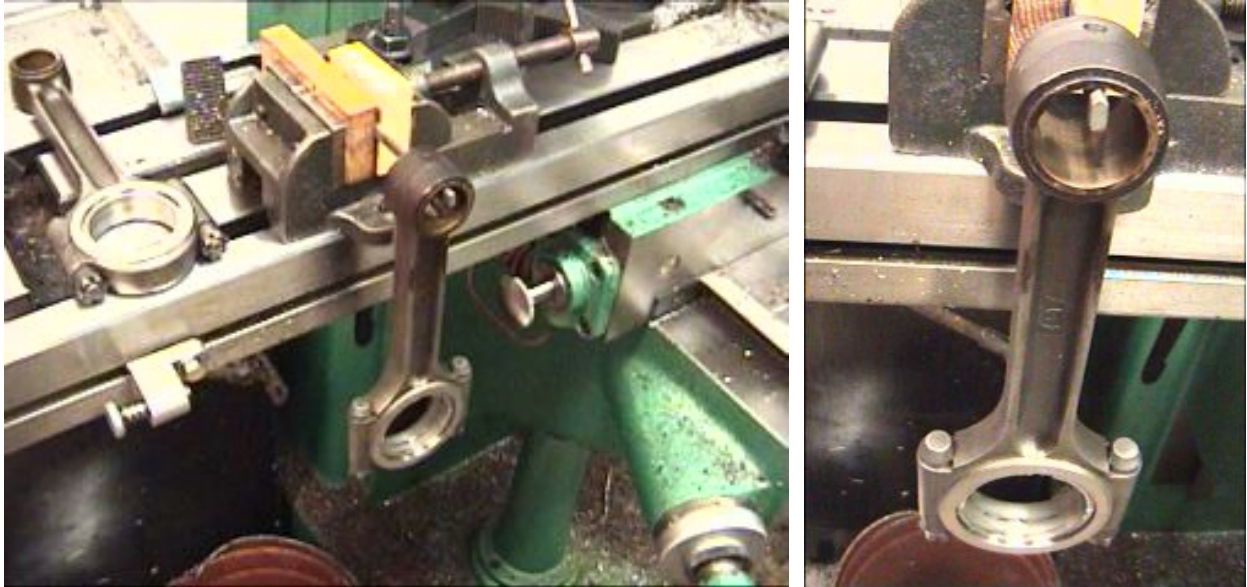


Figure F-6: Connecting rod shown suspended from knife edge for pendulum swing experiment

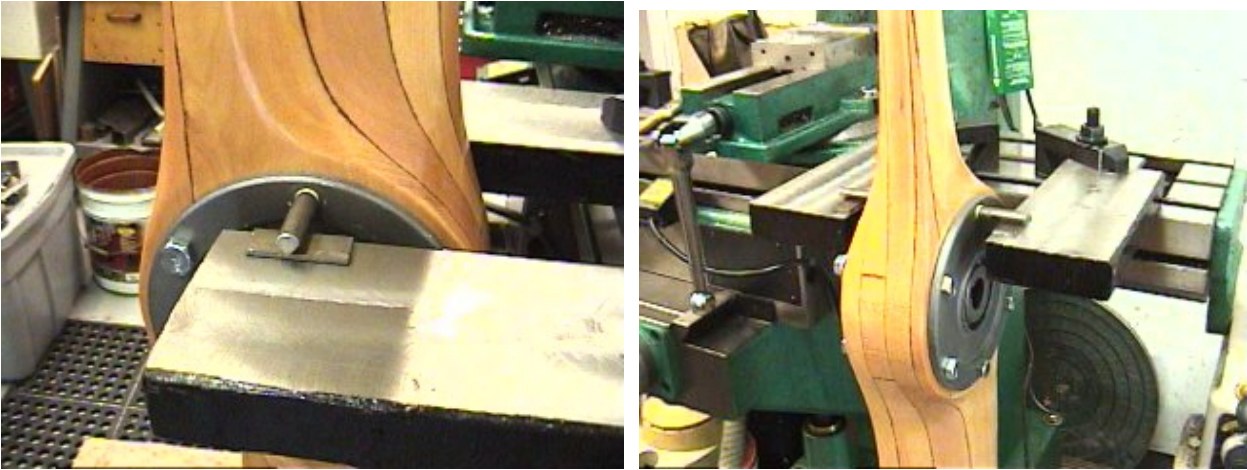


Figure F-7: Propeller knife edge inserted into a prop hub bolt hole

## Vita

Michael Charles Leigh was born in Pennsylvania and was raised in the Pittsburgh area, He studied electrical engineering at Pennsylvania State University and acquired a B.S.E.E. While stationed in Alaska in the U.S. Air Force he acquired a private pilot's license, an FAA Airframe Mechanics license, and an FCC Radiotelephone license. As a flight test instrumentation engineer, he works on both helicopter and airplane test programs. He is also a vintage aircraft enthusiast, machinist, welder, and parts manufacturer involved in the restoration of the Aeronca C-3 airplanes.